Chk1 dynamics in G2 phase upon replication stress predict daughter cell outcome

Vicente Lebrec, Marion Poteau, Jean-Philippe Morretton, Olivier Gavet

Version of Record: https://www.sciencedirect.com/science/article/pii/S153458072200079X
Manuscript_52d4ca4018cd955402ac7ecf5d31e5d6

Chk1 dynamics in G2 phase upon replication stress predicts daughter cell outcome

Vicente Lebrec [2, 3], Marion Poteau[2], Jean-Philippe Morretton[2, 4] and Olivier Gavet[1, 2] *

[1] Sorbonne Universités, UPMC Paris VI, UFR927, Paris, F-75005, France

[2] UMR9019 CNRS, Université Paris-Saclay, Gustave Roussy Cancer Campus, Villejuif, 94805 Cedex, France

[3] Present address: Division of Cancer Biology, The Institute of Cancer Research, 237 Fulham Road, London SW3 6JB, UK.

[4] Present address: INSERM U1279, Université Paris-Saclay, Gustave Roussy Cancer Campus, Villejuif, 94805 Cedex, France

* Lead contact: Dr. Olivier Gavet

Olivier.gavet@gustaveroussy.fr

Running title: Chk1 activity profiles underlie cell outcome

Keywords: replication stress, cell cycle recovery, checkpoint adaptation, checkpoint kinase 1, FRET biosensor

Abbreviations: DRC (DNA replication checkpoint), ssDNA (single-stranded DNA), DSB (double-strand break), RS (replication stress), FRET (Förster Resonance Energy Transfer), NEBD (Nuclear Envelope Breakdown), ATR (Ataxia telangiectasia and Rad3-related protein).

Summary

In human cells, ATR/Chk1 signaling couples S phase exit with expression of mitotic inducers and prevents premature mitosis upon replication stress (RS). Nonetheless, under-replicated DNA can persist at mitosis, prompting chromosomal instability. To decipher how the DNA replication checkpoint (DRC) allows cells to enter mitosis over time upon RS, we developed a FRET-based Chk1 activity sensor. During unperturbed growth, a basal Chk1 activity is sustained along S phase and relies on replication origin firing. Incremental RS triggers stepwise Chk1 over-activation delaying S-phase, suggesting a rheostat-like role of DRC coupled to the replication machinery. Upon RS, Chk1 inactivates as DNA replication terminates but surprisingly reactivates in a subset of G2 cells, which relies on Cdk1/2 and Plk1 and prevents mitotic entry. Yet, active Chk1 is overridden to drive mitosis onset, revealing checkpoint adaptation. Cell division following Chk1 reactivation in G2 results in a p53/p21-dependent G1 arrest, eliminating daughter cells from proliferation.

Introduction

Human cell commitment to mitosis must be strictly coordinated with the completion of DNA replication to maintain the integrity of the genetic content transmitted across cell divisions. Signaling events and regulation of protein expression connect the decision to enter mitosis with the achievement of DNA replication (Lemmens and Lindqvist, 2019). Indeed, abrupt CyclinB1-Cdk1 activation in G2 phase sets up entry into mitosis and is dependent on upstream Polo-like kinase 1 (Plk1) (Gavet and Pines, 2010; Gheghiani et al., 2017). Plk1 activation during G2 requires its phosphorylation by upstream acting Aurora-A kinase and its co-activator Bora (Macůrek et al., 2008; Seki et al., 2008; Tavernier et al., 2021). Phosphorylated form of Bora is needed for Aurora-A activation and relies on CyclinA2-Cdk, an S phase-promoting factor, whose overall kinase activity increases during S/G2 progression together with its cytoplasmic accumulation from G2 onset, Bora being exclusively cytoplasmic (Merrick et al., 2008; Pagano et al., 1992; Tavernier et al., 2021; Vigneron et al., 2018; Zerjatke et al., 2017). Additionally to these signaling events, expression levels of Aurora-A, Plk1 and CyclinB1, increase promptly around G2 onset through Forkhead box protein M1 (FoxM1) transcription factor, whose activity is stimulated by CyclinA2-Cdk (Akopyan et al., 2014; Laoukili et al., 2008). Together, it supports that tight regulation of CyclinA2-Cdk activity level promotes the ordered execution of S and M phases (Gong et al., 2007; Hégarat et al., 2020).

Several studies suggest that the ATR/Chk1 pathway, a main component of the DNA damage response, is active during S phase and in turn modulates CyclinA2-Cdk activity. Interestingly, ATR-dependent γ-H2AX foci were reported during unperturbed S phase, peaking in mid-S, and possibly reflecting DNA damage during replication (Saldivar et al., 2018). Inhibition of ATR or Chk1 in S phase cells induces extra origin firing, partially reversed by Cdk inhibition (Buisson et al., 2015; Eykelenboom et al., 2013; Maya-Mendoza et al., 2007; Petermann et al., 2010a). Consistently, inducible degradation of endogenous Chk1 stabilizes Cdc25A, the main Cdk activating phosphatase in S phase (Goto et al., 2019) and ATR/Chk1 inhibition results in increased phosphorylation of a Cdk2 activity reporter (Daigh et al., 2018). Importantly, ATR

inhibition promotes Cdk-dependent FoxM1 phosphorylation and earlier CyclinB1 expression in S phase associated with premature mitotic entry (Saldivar et al., 2018), supporting the model that DNA replication actively prevents the expression/activation of mitotic inducers and commitment to mitosis. Consistently, the kinetics of mitotic entry is significantly accelerated when S phase is abrogated (Lemmens et al., 2018). However, it remains unknown how the activity of the ATR/Chk1 pathway fluctuates during a several hours long S phase as well as the nature of the molecular events triggering its activation.

Replication fork progression can face threats from various origins, leading to situations referred to as replication stress (RS). RS is commonly observed in precancerous and tumor lesions and is a driver of chromosome instability (Burrell et al., 2013). Cell response to RS relies on ATR-Chk1 pathway, which delays cell cycle progression and allows firing of dormant origins rescuing dysfunctional forks (Ciardo et al., 2019). Contrasting with the expectation that cell cycle progression will only resume after DNA replication is complete, under-replicated DNA can persist at mitosis following RS, even in DRC-proficient cells (Wilhelm et al., 2019). Mitotic under-replicated DNA favor chromosome breakage, notably at common fragile sites (CFSs), and chromosome misegregation (Debatisse and Rosselli, 2019; Wilhelm et al., 2019). How cells achieve mitotic entry in spite of persistent under-replicated DNA and a functional DRC remains a main unanswered question. Among possible scenarios, under-replicated DNA might not trigger DRC activation below a certain threshold amount (Koundrioukoff et al., 2013) or cells might ultimately bypass DRC to enter prematurely into mitosis, a process referred to checkpoint adaptation (Syljuåsen, 2007; Syljuåsen et al., 2006; Toczyski et al., 1997; Yoo et al., 2004).

Here, we develop a FRET-based Chk1 activity sensor and report that Chk1 activation is sustained along the entire non-perturbed S phase and intrinsically relies on replication origin firing. Upon incremental RS, a stepwise Chk1 over-activation takes place and persists up to a genuine S/G2 transition, which allows the expression of mitotic inducers. Strikingly, single cell recordings reveal that Chk1 re-activates in G2 phase functionally preventing mitosis onset, but with a considerable cell-to-cell heterogeneity. Chk1 reactivation in G2 strictly relies on

TOPBP1/ATR and both Plk1 and Cdk1/2 activities, suggesting re-activation is due to activation of G2-specific DNA repair mechanisms. Whereas Chk1 reactivation can be transient, it also persists up to mitosis onset in a subset of dividing cells and becomes predominant upon stringent RS, implying checkpoint adaptation. Notably, both Chk1 reactivation profiles during G2 translate in a high probability of p53/p21-dependent cell cycle withdrawal in G1 daughter cells, thus eliminating checkpoint-reactivating cells from the proliferating cell population.

Results

Development of a FRET-based Chk1 activity sensor

We aimed to characterize Chk1 activity dynamics during unperturbed cell growth and upon genotoxic stresses in live cell assays. We designed a FRET-based phosphorylation sensor to be used as a Chk1 pseudo-substrate, evaluating several Chk1 target sequences (**Figure 1A**)(Blasius et al., 2011; Gheghiani and Gavet, 2016). As Chk1 protein localizes to chromatin and dissociates into the nucleoplasm upon activation (Smits et al., 2006), FRET constructs were targeted to the nucleoplasm using a SV40 NLS motif. Fluorescent nuclear signal was used for automated single cell tracking, segmentation and FRET quantification of asynchronous cell populations. Screening was based on transient expression in RPE1 cells, recording FRET signals before and upon RS induced by aphidicolin, an inhibitor of the B-family DNA polymerases (Koundrioukoff et al., 2013). Selected construct displayed a FRET dynamic range of up to 80%, with peaking as fast as ~5 min upon aphidicolin addition, showing a high sensitivity to RS (**Figure 1B-C**). FRET changes were fully reversed within minutes upon subsequent Chk1 inhibition, using CHIR-124 compound (2,000-fold selectivity for Chk1 over Chk2 *in vitro*, **Figure 1C and S1A**) (Tse et al., 2007). A comparable reversion of the FRET signal was obtained using other Chk1 inhibitors, which further allowed comparing their relative potency at similar concentrations (**Figure S1A**). The use of a non-phosphorylatable form confirmed that FRET changes relied on the phosphorylation of the selected target sequence (**Figure S1B**). Notably, only a fraction of cells exhibited a FRET response upon aphidicolin treatment (**Figure 1B-C**; compare red and grey lines). To identify this subpopulation, the Chk1 sensor was stably expressed in K-In mRuby-PCNA/+ RPE1 cells to identify cell cycle phases based on proliferating cell nuclear antigen (PCNA) stainings (Leonhardt et al., 2000). Recording asynchronous cell populations, we found that S-phase (PCNA-positive foci) cells, but neither the G1 nor G2 subpopulations, exhibited FRET responses upon aphidicolin addition (**Figure 1D-E**). By contrast, etoposide (topoisomerase II inhibitor) treatment induced a marked FRET response in both S and G2 subpopulations (**Figure 1F**), probably linked to the cell-cycle dependent resection of DNA

double strand breaks (DSBs) (Huertas and Jackson, 2009). Deepening the specificity of the Chk1 sensor, we found that its phosphorylation upon aphidicolin or etoposide treatment was reversed by inhibitors of Chk1 (CHIR-124) or upstream acting ATR (AZD6738), but not of Chk2 (PV1019) kinase (**Figure 1G-H & S1C**). Consistent with a requirement of ATM in promoting ATR activation following DSB induction (Jazayeri et al., 2006), Chk1 activation upon etoposide treatment was partially reverted by ATM (KU55933) inhibition (**Figure S1C**). Conversely, ATMi triggered no reversion of Chk1 activity upon aphidicolin treatment (**Figure 1G**). Immunoblots confirmed that ATR, ATM, Chk1 and Chk2 inhibitors suppressed the phosphorylation of Chk1 S345 and Chk2 T68 activating sites and the auto-phosphorylation of Chk1 S296 and Chk2 S516 sites, respectively (**Figure S1D**). We also tested hydroxyurea (HU), an inhibitor of the ribonucleotide reductase, or an excess of thymidine as alternative sources of RS. Both treatments induced a comparable FRET response as upon aphidicolin, but after a reproducible ~10 minutes lag period (**Figure S1E**), likely reflecting the time required to affect nucleotide pools. We conclude that the sensor we developed, hereafter referred to as Chk1 activity sensor, is specifically phosphorylated upon Chk1, but not Chk2, activation and is ideally suited to monitor ATR/Chk1 signaling in live cell assays.

DNA replication *per se* sustains basal Chk1 activity along S phase

To better understand how a tight coordination between completion of DNA replication and commitment to mitosis is achieved during unperturbed cell growth, we examined Chk1 activity dynamics along the entire cell cycle. Asynchronous mRuby-PCNA/+, Chk1 sensor RPE1 cells were recorded and S phase onset was defined by the appearance of uniformly distributed small replication (PCNA-positive) foci or by the increase of mRuby-PCNA expression as a surrogate marker (Zerjatke et al., 2017). The disappearance of broad PCNA foci was used to identify the S/G2 transition (Leonhardt et al., 2000). Chk1 activity was minimal during G1, and progressively built up for ~2 hours after the initiation of PCNA expression, reaching a maximum level that slowly declined along S phase progression (**Figure 2A, left panel**). Chk1 activity then dropped

in the last hour before the S/G2 transition to reach a minimal G1-like level during G2 that persisted up to mitosis onset (**Figure 2A, central panel**). A transient FRET variation was observed immediately following NEBD (**Figure 2A, right panel**), but was also present in cells expressing the non-phosphorylatable form (**Figure S2A**), indicating that it does not originate from sensor phosphorylation. Identical Chk1 activity profile along the cell cycle was observed in non-genetically modified hTert-RPE1 (ECACC) cells, ruling out that Chk1 activity detected in S phase was due to perturbations of DNA replication caused by the mRuby cassette integration at the PCNA locus (**Figures S2B**). Interestingly, we observed higher and more variable Chk1 activity levels during S phase progression in osteosarcoma U2OS cells (mean ΔFRET∼35% in U2OS cells with highest ΔFRET values ∼70%, versus ΔFRET∼25% in RPE1 cells) possibly reflecting a constitutive RS in these cells (**Figure S2C**). Using Chk1 sensor fused to histone protein H2B, we found that local Chk1 activity dynamics at chromatin was undistinguishable to the one recorded in the nucleoplasm, although the maximal extent of H2B-Chk1 sensor FRET signal in S phase was slightly reduced (**Figure S2D**). Because the increase of PCNA expression at the G1/S transition might significantly precede the activation of replication origins *per se* (Zerjatke et al., 2017), we carefully compared Chk1 activity fluctuations with the appearance of PCNA-positive replication foci. A close temporal correlation was observed at S phase onset between Chk1 activity increase and sudden PCNA foci appearance (**Figure S2E**), as well as at S/G2 transition between Chk1 inactivation and foci disappearance (**Figure S2F**).

To unravel the origin of Chk1 activation along S phase, asynchronous cells were treated with a DDK (Dbf4-dependent Cdc7 kinase) inhibitor (XL-413), which inhibits Mcm2-7 phosphorylation and DNA replication during S phase (Alver et al., 2017; Yamazaki et al., 2012). Chk1 activity was steeply suppressed upon Cdc7i with comparable kinetics between early, mid and late S phase cells (**Figure 2B**). The duration of the Chk1 inactivation kinetics upon Cdc7i (∼45-60 min; **Figure 2B**) agree with the measured average lifetime of active replication foci (Chagin et al., 2016) and is closely similar to the one observed at the S/G2 transition (**Figure S2G**). We ruled out that Chk1 inactivation upon Cdc7i was due to a requirement of DDK to fully activate Chk1, as

previously reported upon replication fork stalling (Sasi et al., 2018). Indeed, aphidicolin addition in the next hour following Cdc7i induced a *de novo* increase of Chk1 activity (**Figure 2C, left and central panels**), demonstrating that the kinetics of Chk1 activation upon fork stalling is not affected by Cdc7 inhibition. To confirm that Cdc7 inhibition mainly reduces Chk1 activity through the suppression of new origin firing, cells were pretreated for an hour with aphidicolin before Cdc7i. As local dormant origin firing occurs within the first ~30 min upon RS (Courbet et al., 2008) whereas distant origin firing is otherwise inhibited (Técher et al., 2017), inhibition of Cdc7 one hour after RS induction is expected not to further reduce new origin firing. Indeed, aphidicolin treatment resulted in rapid Chk1 activation, but subsequent Cdc7 inhibition had no effect on Chk1 activity level (**Figure 2C, right panel**).

We addressed the mechanisms responsible for Chk1 activation at active replication origins. Chk1 activity increase following S phase entry was unaffected by the addition of dinucleotide (dNTP) precursors (**Figure S2H**), suggesting that Chk1 activation during S phase is not linked to a dNTP pool shortage, as reported in budding yeast (Forey et al., 2020). Two ATR-activating proteins ETAA1 and TOPBP1 have been identified and are differentially recruited to chromatin. While ETAA1 directly interacts to RPA bound to single-stranded DNA (ssDNA) (Lee et al., 2016), a 5'-ended ssDNA-dsDNA junction is required for TOPBP1-mediated ATR activation (Duursma et al., 2013). Transient ssDNA and 5'-ended primers are generated on the lagging strand of each ongoing replication fork. We found that depleting TOPBP1 strongly suppressed Chk1 activity along the entire S-phase (**Figure 2D & S2I)**. While ETAA1 depletion alone did not significantly affect Chk1 activity, a small additive effect was observed upon TOPBP1 and ETAA1 co-depletion (**Figure 2D**). Altogether, our results show that Chk1 activation occurs all along unperturbed S phase and strongly suggest that it inherently relies on the activation of replication origins. Hence, it supports the conclusion that activation of DRC is intrinsically linked to the DNA replication process *per se*.

Chk1 activity level in S phase is exquisitely sensitive to RS intensity

How under-replicated DNA can persist at mitosis upon RS in DRC-proficient cells, challenging chromosome integrity, remains puzzling. Previous work suggested that a mild RS could be insufficient to trigger the activation of Chk1-dependent DRC (Koundrioukoff et al., 2013). We addressed the putative existence of an activation threshold. Aphidicolin treatment on S phase cells immediately stimulated Chk1 basal activity, whereas on G1 cells it was followed by a higher Chk1 activity at S phase onset (**Figure 3A**). Using incremental aphidicolin doses (from 0.03 to 2 µM), which gradually affect replication fork progression (Koundrioukoff et al., 2013), Chk1 activity in S phase cells rapidly increased, even at the lowest dose used, and reached a near steady state after a few dozen minutes. In all conditions, Chk1 activity was reversed to a G1-like state upon Chk1i (**Figure 3B**). We found that the Chk1 activity level reached at near-steady state was linearly related to RS intensity (**Figure 3C**). Investigating local Chk1 activation at chromatin provided similar observations (**Figure S3A**). We considered the possibility that Chk1 activation upon RS might be differentially modulated along S phase, but we observed identical Chk1 activation kinetics in early, mid and late S with a maximum FRET signal reached ~4min after drug addition (**Figure S3B**). We analyzed the mechanisms at stalled forks that lead to abrupt Chk1 activation. While ETAA1 depletion had hardly any effect, TOPBP1 knock down fully suppressed Chk1 over-activation upon aphidicolin treatment (**Figure 3D**). Hence, it suggests that the formation of ssDNA stretches due to uncoupling of helicase and DNA polymerase activities might not be sufficient for Chk1 over-activation and also requires 5'-ended ssDNA-dsDNA junctions (Van et al., 2010). Consistently, addition of an inhibitor of polymerase primase alpha (POLA1), previously shown to induce extended ssDNA formation at fork junctions (Ercilla et al., 2020), induced in S phase cells a slow and gradual Chk1 activity increase over time (**Figure S3C**), in sharp contrast to the abrupt activation upon aphidicolin (**Figure 3B**). Together, our results argue against a limited sensitivity of the ATR/Chk1-dependent DRC to fork stalling as a possible explanation for mitotic entry despite persistence of under-replicated DNA. Also, it suggests that similar mechanisms are responsible for Chk1 activation during unperturbed S phase and upon RS.

G2 cells exhibit different Chk1 activity profiles related to RS stringency

We analyzed the kinetics of mitotic entry upon incremental RS and the modulations of Chk1 activity during cell cycle resumption. Phase contrast imaging showed that after a reproducible lag period of ~2.5 hours, fitting with G2 phase duration in RPE1 cells, entry into mitosis of asynchronous cells was progressively delayed from 0.1 to 2μM aphidicolin doses (**Figure S4A**), consistent with stepwise Chk1 over-activation observed. Notably, even under the strongest RS condition, a small subset of cells reached mitosis up to 20h after treatment (**Figure S4A**). We monitored cell cycle phase transitions using mRuby-PCNA staining upon moderate to stringent RS. Most S-phase cells were delayed or arrested upon treatment and the proportion of cells that reached S/G2 transition, defined by stereotypical late S broad PCNA foci disappearance, decreased in relationship to RS intensity (**Figure S4B, left**). Most of these cells remained arrested in G2 and only a subset entered mitosis and divided (from 7 to 2.5% of the whole cell population from 0.3 to 1 μM aphidicolin, respectively) (**Figure S4B, right**). No cell entered mitosis in the absence of a detectable G2 phase.

Chk1 inactivation was invariably taking place in each cell reaching the S/G2 transition under RS (**Figure 4A**), and closely correlated with PCNA foci disappearance (**Figure S4C**). While the time needed for Chk1 inactivation at the S/G2 transition increased with RS intensity as expected, the rate of Chk1 inactivation was closely similar between untreated and aphidicolin-treated cells (**Figure S4D-E**). We confirmed that PCNA foci disappearance upon RS corresponds to a genuine S/G2 transition by recording endogenous Plk1 protein levels. Indeed, expression of Plk1 initiated at the S/G2 transition during unperturbed cell cycle (Akopyan et al., 2014), was reproducibly taking place shortly after PCNA foci disappearance upon RS, with relative kinetics undistinguishable from untreated conditions (**Figure S4F**).

Unexpectedly, individual cells displayed heterogeneous Chk1 activity profiles during the G2 phase immediately following RS. First, among cells that reached mitosis and divided, three different G2 phase Chk1 profiles could be defined: (i) no significant Chk1 reactivation up to mitosis (referred to as 'no Chk1 reactivation'), (ii) a transient reactivation that ended-up shortly

before entry into mitosis ('transient Chk1 reactivation'), and (iii) a Chk1 reactivation profile that persisted up to prometaphase onset (NEBD) ('persistent Chk1 reactivation') (**Figure 4A-B**). Second, among cells that remained arrested in G2 ('No M phase'), Chk1 did not reactivate or a transient reactivation was rapidly initiated after the S/G2 transition for up to ~6h duration (**Figure 4C**). Chk1 reactivation during G2 was not restrained to RPE1 cells and was also observed in U20S cells during cell cycle resumption upon RS (**Figure S5A-B**).

Among dividing cells, the relative proportions of the three G2 phase-Chk1 activity profiles were related to RS intensity. Indeed, the fraction of cells exhibiting no Chk1 reactivation progressively decrease to the benefit of the two others upon increasing aphidicolin doses (from 50% at 0.3 μM to 15% at 1 μM aphidicolin), and upon 1 μM aphidicolin the majority of cells entered into mitosis despite persistent Chk1 activity (**Figure 4D**). G2 phase-Chk1 activity profiles were also related to the time duration spent in S phase upon aphidicolin treatment before the S/G2 transition. 'No Chk1 reactivation' was predominant in the first wave of cells that reached G2 phase upon RS (**Figure 4E and S5C, green lanes**), while cells that exhibited both Chk1 'reactivation' profiles spent a longer time in S phase (**Figure 4E and S5C, red and purple lanes**).

To summarize, higher exposure to RS during S phase, either through higher doses of aphidicolin or by increased time spent in S phase upon perturbed DNA replication, translates to a higher probability of Chk1 reactivation during the following G2 phase.

p53 drives permanent arrest and silencing of the ATR/Chk1 pathway in G2 phase

We determined that cells spending the longest resident time in S phase upon RS remained arrested in G2 phase, with either a transient or no Chk1 reactivation (**Figure 4E and S5C**, "no M-phase", purple and grey lanes). Untransformed cells can irreversibly exit cell cycle in G2 phase upon DNA damage insult, which is primarily determined by ATR/Chk1 signaling and relies on induction of p53 (Bunz et al., 1998; Hastak et al., 2008; Krenning et al., 2014). We suspected that the time-dependent distribution of the Chk1 profiles in G2 might be, at least partially, driven by

the kinetics of p53 activation upon RS. Depletion of p53 caused the majority of cells that reached S/G2 transition to enter into mitosis, from ~50% of cells in control to >80% upon p53 depletion (**Figure 5A & S5D**), consistent with a previous report (Barr et al., 2017). Remarkably, this was accompanied by a marked increase of G2 cells exhibiting Chk1 reactivation, whereas the percentage of G2 cells with no Chk1 reactivation remained constant (**Figures 5B and S5E**). We performed the opposite experiment by treating cells with high dose of aphidicolin to maximize the probability of Chk1 reactivation in G2 phase, then stabilizing p53 using the MDM-2 inhibitor Nutlin-3a (Vassilev et al., 2004). Around 4h after Nutlin-3a treatment, entry into mitosis was completely inhibited, consistent with previous findings (Krenning et al., 2014). Importantly, cells in S phase at the time of Nutlin-3a treatment massively did not re-activate Chk1 in the subsequent G2 phase (**Figure 5C**, green and grey lanes). Neither p53 depletion nor addition of Nutlin-3a affected Chk1 activity in S phase (**Figure S5E-F)**, indicating p53 modulation of Chk1 activity is restrained to G2 phase. Collectively, our results suggest that during cell cycle resumption and related to the duration and intensity of RS before S/G2 transition, cells bifurcate between two outcomes at S/G2 onset: (i) No or low initial p53 induction and the competence to re-activate Chk1 during G2 phase, or (ii) high initial p53 induction promoting Chk1 activity silencing early on during G2 and cell cycle exit.

Chk1 re-activation during G2 relies on Cdk1/2 and Plk1-dependent repair mechanisms

We addressed the mechanisms promoting Chk1 re-activation in a subset of G2 cells despite the lack of reappearance of PCNA positive replication foci. Chk1 activity in G2 phase remained dependent on ATR and was unaffected by ATMi or Chk2i, nor by Cdc7i, arguing against *de novo* origin firing (**Figure 5D & S6A-C**). Upon RNAi, cells with suppressed Chk1 activity in S phase due to efficient TOPBP1 depletion did not reactivate Chk1 during the next G2 phase, supporting that Chk1 reactivation in G2 also relies on TOPBP1 (**Figure 5E**). We hypothesized that ATR-dependent Chk1 re-activation might rely on ssDNA tracks generated during G2 by timely activated post-replicative repair mechanisms. Consistently, we observed that PARP inhibition

(olaparib) did not modify Chk1 activity in S phase but specifically affected its re-activation in G2 (**Figure 5F**). Cyclin-Cdk2 and -Cdk1 activity levels rise during S/G2 progression (Goldstone et al., 2001; Merrick et al., 2008; Pagano et al., 1992) and promote both DNA end resection events and homology-directed repair pathways through the phosphorylation of several repair factors (Lim et al., 2020; Palermo et al., 2016; Tomimatsu et al., 2014; Trovesi et al., 2013; Yata and Esashi, 2009). We found that Chk1 reactivation in G2 phase is strongly dependent on both Cdk2 and Cdk1 activities (**Figure 5G**). We tested whether inhibition of either Plk1, identified in the late response to stalled forks (Xu et al., 2017), or ATM, an upstream regulator of the DSB response, affect Chk1 reactivation. Because a previous work suggested that homology-directed repair pathways might be less efficiently inhibited once initiated (Huang et al., 2012), ATMi or Plk1i (BI2536) were added within 2h following aphidicolin treatment. While ATMi had hardly any effect (**Figure S6D**), Plk1i strongly affected Chk1 activity profiles in G2 (**Figure 5H & S6E**). First, the fraction of cells exhibiting a persistent Chk1 reactivation up to NEBD was fully abolished upon Plk1i (**Figure S6E-F**). Second, the rate of Chk1 reactivation during G2 was markedly slowed down, independently of the cell ability to enter or not into mitosis, providing evidence that Plk1 is directly involved in the mechanisms promoting Chk1 reactivation (**Figure 5H & S6E**). The fraction of cells exhibiting Chk1 reactivation decreased from ~65 to 20% upon Plk1i. Plk1 interacts with some DNA repair proteins (BRCA1, BRCA2, SLX4) and phosphorylates Rad51 at stalled forks (Xu et al., 2017; Yata et al., 2012, 2014). In an attempt to determine how Plk1 contributes to Chk1 reactivation in G2, Rad51i (B02) versus Rad52i (AICAR) were added 2h after RS induction. While Rad51i greatly reduced the number of cells that achieved the S/G2 transition by up to ~80%, neither Rad51i nor Rad52i had a significant effect on Chk1 reactivation kinetics in G2 nor on the percentage of G2 cells that reactivated Chk1 (**Figure S6G**). Collectively, our findings support that a TOPBP1/ATR-dependent Chk1 reactivation is initiated in a subset of G2 cells following perturbed DNA replication due to post-replicative repair mechanisms timely activated from G2 onset in a Plk1 and Cdk1/2-dependent manner.

Override of active checkpoint signaling upon RS triggers premature mitosis onset

We were intrigued that a subset of cells entered into mitosis and divided despite a Chk1 reactivation signal that persisted up to NEBD ('persistent Chk1 reactivation'), and considered the possibility that these cells might override active checkpoint signaling. The G2 phase duration in the overall cell population is notably prolonged following RS induction in S phase (**Figure 6A**), and is significantly longer in cells exhibiting either Chk1 reactivation profiles during G2 versus no reactivation (**Figure 6B**), supporting that Chk1 reactivation might delay commitment to mitosis. To assess the contribution of Chk1 activity in G2 phase to checkpoint mechanisms preventing mitosis onset, Chk1i or ATRi were added at a set time during recording. In unperturbed conditions, ATRi laid no effect on G2 phase duration, while Chk1i induced a minimal shortening (Mean G2 duration CT: 180 min; Chk1i: 160 min) (**Figure S6H**). Upon RS, both ATRi and Chk1i treatments immediately suppressed Chk1 activity in G2 cells, which was invariably and rapidly followed by entry into mitosis in all cells analyzed (**Figure 5D and 6C**). Quantification of the time intervals between Chk1i or ATRi treatment versus DMSO and mitosis onset confirmed that inhibition of ATR and Chk1 in G2 cells exhibiting Chk1 reactivation profiles triggered a premature mitotic entry (**Figure 6D**). Chk1i could force mitotic entry up to ~6h after G2 onset, following which no more Chk1 activity could be detected in any persistently arrested G2 cell (**Figure S6I**), suggesting that Chk1 inhibition can trigger mitotic entry during the window of time its activity is detectable. In addition, we found a direct correlation between the level of Chk1 activity in individual G2 cell at drug addition and the kinetics of entry into mitosis upon Chk1i (**Figure S6J**), further supporting that active ATR/Chk1 signaling during G2 prevents unscheduled mitosis upon RS. We conclude that during cell cycle resumption a subset of cells override active ATR/Chk1 signaling to prematurely enter mitosis, providing a direct observation of checkpoint adaptation in human cells upon RS.

Cell division following Chk1 reactivation during G2 results in G1 arrest of daughter cells

We examined the outcome of daughter cells originating from mother cells exhibiting either Chk1 reactivation profile during G2. Dividing cells upon moderate RS (aphidicolin 0.5 μM) were followed over the next cell cycle, and both the reappearance of replication (PCNA-positive) foci and increase of Chk1 activity used to identify cells re-entering into S phase. No second mitosis was observed during long-term recordings (>48h), certainly as a consequence of the continuous presence of aphidicolin that will affect the whole duration of the second S phase. Re-entry into S phase during the second cell cycle was massively taking place among daughter cells originating from a mother cell without Chk1 reactivation during G2 (**Figure 6E**). Conversely, the vast majority of daughter cells originating from a mother cell exhibiting either Chk1 reactivation profile during G2 remained permanently arrested in G1 (**Figure 6E**). P53 and p21 knockdown massively alleviated the permanent G1 arrest of these latter subpopulations (**Figure 6F**). Thus, Chk1 reactivation during G2, following perturbed DNA replication in S phase, translates in a high probability of p53/p21-dependent proliferation withdrawal in the next G1 phase in untransformed human cells.

Discussion

Maintenance of genome integrity across cell divisions is instrumental for cell survival, identity and fate. Duplication of large genomes within the few hours-long S phase represents a peculiar challenge as it can be perturbed by a variety of situations referred to RS. In spite of ATR/Chk1-dependent DRC signaling delaying S phase and compensation mechanisms, RS is a recognized source of genetic instability early on during tumorigenesis (Tsantoulis et al., 2008). Here, we develop a FRET-based Chk1 sensor and report that Chk1 exhibits a sustained basal activity all along unperturbed S phase. We provide evidence that it originates from the activation of replication origins *per se*, while it remains to discriminate whether Chk1 activity level at any time is the result of thousands of elongating forks or is due to the stochastic stalling of a subset of forks. Interestingly, Chk1 activity correlates with the amount of ongoing forks in *Xenopus* egg extracts (Murphy and Michael, 2013). Upon incremental RS, a stepwise Chk1 over-activation is taking place gradually delaying S phase, supporting that ATR/Chk1-dependent DRC works like a rheostat intrinsically coupled to the replication machinery. Following S phase exit under RS, single-cell analyses reveal unanticipated heterogeneous Chk1 activity profiles during the following G2 phase. Strikingly, in spite of a sustained Chk1 reactivation profile during G2 that functionally prevents mitosis onset, a subset of cells ultimately achieves entry into mitosis. This checkpoint override or adaptation becomes prominent upon incremental RS. Hence, our data suggest that checkpoint adaptation is a driving mechanism for the persistence of under-replicated regions at mitosis upon RS, and might contribute to gross chromosome rearrangements observed in cancer cells (Burrell et al., 2013; Kalsbeek and Golsteyn, 2017).

We found that depletion of the ATR co-activator TOPBP1 strongly reduces Chk1 activity in S phase during normal cell growth, in opposition to ETAA1 knockdown. This result seems contradictory with a previous finding that ATR-dependent phosphorylation of DNA damage marker H2AX observed in some S phase cells and peaking in mid-S, relies on ETAA1 (Saldivar et al., 2018). However, ETAA1 and TOPBP1 co-activators confer distinct substrate specificity to

ATR (Bass et al., 2016; Haahr et al., 2016), providing a possible explanation for the discrepancy between these observations.

Upon stringent RS, the slowing down of replication forks might be expected to drive DNA replication overlapping with the G2 phase and persisting up to mitosis onset, consistent with the presence of replication intermediates, notably at CFSs, during mitosis (Debatisse and Rosselli, 2019). Contrary to this model, a several hours long G2 phase is invariably taking place in each individual cell during cell cycle resumption upon RS and allows the accumulation of mitotic inducers, such as Plk1, that trigger mitotic entry (Gheghiani et al., 2017). Hence, the expression of mitotic inducers is controlled in a similar way by ATR/Chk1 signaling in normal growth conditions and upon RS ensuring the maintenance of the temporal uncoupling between DNA replication and commitment to mitosis.

Following perturbed DNA replication in S phase, Chk1 re-activates in a subset of G2 cells. Our results suggest that Chk1 re-activation relies on some post-replicative DNA repair mechanisms timely activated during G2. Indeed, Chk1 re-activation depends on Cdk1/2 whose activities build up during S/G2 progression and strongly relies on Plk1, while Chk1 activity in S phase remain unaffected by Plk1 inhibition. Chk1 reactivation relies on TOPBP1 and ATR suggesting DNA strand resection during G2. Different post-replicative DNA repair processes working either alone or in combination might be responsible for G2 phase Chk1 reactivation, including (i) resection/filling of ssDNA gaps left behind by replication forks upon RS (Lopes et al., 2006; Tirman et al., 2021; Zellweger et al., 2015) and/or (ii) nuclease-mediated homology-directed repair (HR; Break-Induced Replication) of collapsed forks (Ait Saada et al., 2018; Minocherhomji et al., 2015; Petermann et al., 2010b). Future investigation are required to characterize the underlying mechanisms.

The persistence of chromosome aberrations at mitosis, such as gaps and breaks, upon genotoxic stresses provided indirect evidence of checkpoint "adaptation" (Syljuåsen, 2007). Here, we found that Chk1 reactivation during G2 underlines functional checkpoint signaling preventing a premature mitotic entry. Yet, both untransformed and cancerous human cells could enter

mitosis despite persistent high Chk1 activity, providing a direct observation of checkpoint override. We determined that checkpoint override upon RS is crucially dependent on Plk1 activity, consistent with some previous findings (Syljuåsen et al., 2006; Toczyski et al., 1997; Yoo et al., 2004). Importantly, we observed no sign of Chk1 activity attenuation up to mitotic entry that might have primed the transition into mitosis, in contrast to the transient Chk1 activity profile observed in some G2 cells that support checkpoint recovery (Bartek and Lukas, 2007). Hence, Plk1-mediated inactivation of Chk1 is not required for checkpoint override and both kinases probably act in parallel to control mitotic entry. Plk1 might counteract the inhibition of Cdk activating phosphatases Cdc25s by Chk1 through Wee1 degradation (Watanabe et al., 2005), or integration of Plk1 and Chk1 phosphorylation events on Cdc25s might promote mitotic entry. Consistently, we previously identified Plk1 phosphorylation sites stimulating Cdc25C activity (Gheghiani et al., 2017).

During cell cycle resumption upon RS, dividing cells that re-activated Chk1 in the preceding G2 phase massively arrest in the next G1 through a p53/p21 dependent mechanism. Because both G2 and G1 arrest are p53-dependent and related to RS exposure, we speculate that stalled/collapsed forks early on during S phase might initiate precocious p53 accumulation leading to a protein level sufficient to trigger cell cycle withdrawal in G2, while transmission of a p53 pool whose accumulation was initiated later during S/G2 progression or transmission of under-replicated/damaged DNA might promote cell cycle withdrawal in the next G1 phase. We favor the former scenario, as we did not find any correlation between the number of 53BP1 nuclear bodies observed in G1 daughter cells and G2 phase Chk1 activity profiles in mother cells (**Figure S6K**). Consistently, p53 and p21 accumulation initiated in mother cells was shown to contribute to cell cycle decision by daughter cells (Barr et al., 2017; Yang et al., 2017). G2 or G1 phase cell cycle withdrawals will ensure that cells experiencing significantly perturbed DNA replication, followed or not by checkpoint adaptation, will not propagate altered genomes.

Replication stress is a major source of genetic instability in cancer cells and sustained DRC activation was proposed to act early on as a barrier to tumorigenesis (Bartkova et al., 2005; Hills

and Diffley, 2014). Dissecting the regulation and complex interplay between anti- and pro-mitotic signaling pathways will help to understand how genetic alterations can be initially established in checkpoint-proficient non-tumoral cells.

Limitations of the study

The development of a FRET-based Chk1 sensor combined with live single cell imaging assays allowed us to identify subpopulation of cells exhibiting different Chk1 reactivation profiles during the G2 phase immediately following RS that predict G1 daughter cell outcome. The requirement to record the entire G2 phase for classification and the fact that the different subpopulation of cells reached mitosis with distinct timings precluded most biochemical or immunofluorescent assays at fixed time points on asynchronous cell populations. As such, genomic screening and development of tunable genetically engineered perturbation tools will be required to decipher the molecular machinery driving Chk1 reactivation in G2 phase.

Acknowledgements

We thank Dr. Gerard Mazon and Dr. Daniele Fachinetti for critical reading of the manuscript. This project was funded by the Agence Nationale de la Recherche (ANR-17-CE13-0011-03). V.L was supported by the "IDI 2015" project funded by the IDEX Paris-Saclay (ANR-11-IDEX-0003-02) and Ligue Nationale Contre le Cancer (IP/SC-15956).

Author contributions

O.G conceived the project and designed experiments with V.L. V.L performed experiments. M.P contributed to knock down experiments and J.P.M developed stable cell lines. O.G and V.L wrote the manuscript.

Declaration of interests

The authors declare no competing interest.

MAIN FIGURES

Figure 1: Development of a FRET-based Chk1 activity sensor

(**A**) Outline of the FRET-based Chk1 activity sensor. Phosphorylation of Chk1 substrate sequence induces binding to a phospho-binding domain (green), resulting in a conformational change and a decrease of FRET between CFP and YFP variants.

(**B**) Asynchronous RPE1 cells transiently expressing Chk1 sensor were treated with aphidicolin. Red arrow points to a cell exhibiting FRET response to treatment while grey arrows point to cells with no FRET variation.

(**C**) Same as (**B**). Aphidicolin was added at the indicated time point before subsequent addition of Chk1i. Each single cell is plotted. Cells that responded to aphidicolin are in red, others in grey. CFP/YFP ratios, hereafter referred as 1/FRET values, are normalized to last time point.

(**D-F**) FRET variations over time of G1, S or G2 cells upon (D-E) aphidicolin or (F) etoposide addition. Bars, 10 μm. N≥ 2experiments

(**G-H**) FRET variations over time in RPE1 mRuby-PCNA/+ Chk1 sensor cells. Cells were first treated by aphidicolin then by DMSO, Chk1i, Chk2i, ATRi or ATMi. Only the aphidicolin responding (S phase) cells are displayed. Cells that responded to the second treatment are plotted in red, others in grey. Each line represents a single cell, bold curve is mean. N=2

Figure 2: Chk1 activity along S phase relies on replication origin firing

(**A-D**) 1/FRET values over time in asynchronous RPE1 mRuby-PCNA/+ Chk1 sensor cells. Each line is a single cell, bold curve is mean.

(**A**) Bottom: cells were synchronized *in silico* either to PCNA expression (S phase onset), PCNA foci disappearance (S/G2 transition) or nuclear envelope breakdown (NEBD). Up: A representative cell is displayed. Bar, 10 μm. N=3 experiments

(**B**) Cells were treated with Cdc7i to prevent new origin firing. Cells in S phase at the time of inhibitor addition were sorted in three groups based on the time spent in S phase. For each cell displayed, S phase onset, as determined by PCNA expression, is represented as a vertical line. N>3

(**C**) S phase cells were treated with Cdc7i then aphidicolin (0.5 μM), or alternatively aphidicolin then Cdc7i, before subsequent addition of Chk1i. Each single cell is plotted. 1/FRET values are normalized to 50 min after Chk1i. (middle) S phase cells that entered into G2 phase between Cdc7i and aphidicolin are displayed in red. N=3

(**D**) Cells depleted for ETAA1, TOPBP1 or both (48h) were synchronized *in silico* to S/G2 transition. Left panels: cell cycle progression of each cell is displayed by color change (G1 in green, S in blue, G2 in red, M and next G1 in dark green). Right panel: Mean + SEM. N=3

Figure 3: Chk1 activity level in S phase correlates to RS stringency

(**A-D**) Asynchronous RPE1 mRuby-PCNA/+ Chk1 sensor cells. Each line is a single cell, bold curve is mean.

(**A**) Cells were treated with aphidicolin either in S phase (left) or in G1 (right) and 1/FRET variations of each single cell plotted over time. For each cell, S phase onset is indicated as a vertical line. 1/FRET values are normalized to 15 min before S phase onset. N>3

(**B**) Cells were first treated with increasing doses of aphidicolin, then with Chk1i. Only cells that responded to Chk1i are plotted. In red, cells in S phase at t_0 and in purple, cells that entered S phase after aphidicolin addition. 1/FRET values are normalized to after Chk1 inhibition. N=3

(**C**) as in (B). 1/FRET values 1 hour after aphidicolin addition upon increasing doses are plotted. >100 cells per condition. t test: * $p<0.05$, *** $p<0.001$

(**D**) Cells depleted for ETAA1 or TOPBP1 (48h) were treated with aphidicolin then Chk1i. Only cells in S phase at t_0 are plotted.

Figure 4: Chk1 reactivates in G2 phase during cell cycle resumption upon RS

(**A-E**) Asynchronous RPE1 mRuby-PCNA/+ Chk1 sensor cells.

(**A**) Representative gallery of a cell treated in S phase with aphidicolin and exhibiting Chk1 reactivation in the subsequent G2 phase persisting up to mitotic entry (NEBD). Bar, 10 µm

(**B** and **C**) Cells treated with aphidicolin (0.5 µM) in S phase were synchronized *in silico* to S/G2 transition (PCNA foci disappearance) and sorted into five classes: (**B**) Cells that entered mitosis displayed no (left), persistent (middle) or transient (right) Chk1 reactivation during G2 phase; (**C**) Cells that remained arrested in G2 displayed transient (left) or no Chk1 reactivation (right). Color code as in Fig. 2D. In (B), orange color indicates S phase re-entry in the next cell cycle. 1/FRET values are normalized to G2 onset. N>3

(**D**) Proportions of G2 phase Chk1 activity profiles among cells reaching mitosis upon indicated aphidicolin doses. N ≥ 2 experiments per condition.

(**E**) Cell cycle progression and pseudo-color code of Chk1 activity profiles during G2 phase from cells treated with aphidicolin at indicated time (red vertical line) and either progressing to mitosis (NEBD) or not (No M-phase). Each row represents a single cell. Cells are ordered according to the time of S/G2 transition. n= 441 cells from a representative experiment. N=3

Figure 5: Chk1 re-activation in G2 phase relies on Cdk1/2 and Plk1 and is silenced by p53

Asynchronous RPE1 mRuby-PCNA/+ Chk1 sensor cells.

(**A**) Following or not p53 depletion for 24h, cells were treated with aphidicolin at t_0 and recorded over time. Each row represents a single cell. Blue: G2 cells entering into mitosis, orange: G2 cells without mitosis. N=2

(**B**) as in (**A**), proportions of cells displaying Chk1 re-activation (transient or persistent) among the G2 subpopulations that either stay arrested (left) or reaches mitosis (right).

(**C**) Cells were treated with aphidicolin (1 μM) then by DMSO (left) or Nutlin-3a (right). Each row represents a single cell. Chk1 activity profiles in G2 phase are displayed as in Fig. 4E.

(**D**) Cells were treated with aphidicolin in S then with ATRi in G2 phase. 1/FRET values are normalized to G2 onset. Color code as in Fig. 2D. Bold (black) line is mean of all cells in G2 phase (red). N=3

(**E**) Following or not TOPBP1 depletion (24h), cells were treated with aphidicolin (0.5 μM) and 1/FRET recorded over time. Right: Cells with low Chk1 activity in S phase, denoting efficient TOPBP1 depletion, are in blue, others in red. Note that TOPBP1-depleted (blue) cells do not reactivate Chk1 in G2.

(**F**) Cells were treated with aphidicolin then with PARPi 2h later. Cells were synchronized *in silico* to G2 onset and 1/FRET (Mean+SEM) plotted. Cells were gathered in two categories: no Chk1 reactivation in G2, followed or not by mitosis (grey or black curve); Chk1 reactivation (either transient or persistent) in G2, followed or not by mitosis (green or orange). For each condition, proportion of cells re-activating Chk1 in G2 is indicated. N=2

(**G**) Cells were treated with aphidicolin in S then with Cdk1/2i, Cdk1i or Cdk2i in G2 phase. Plotted as in (D). N=3

(**H**) as in (F). Cells were treated with aphidicolin then with Plk1i 2h later. N=2

Figure 6: Chk1 re-activation in G2 translates in a p53/p21-dependent G1 arrest of daughter cells

Asynchronous RPE1 mRuby-PCNA/+ Chk1 sensor cells.

(**A**) Cells were treated with indicated dose of aphidicolin. G2 phase duration is plotted for all cells entering mitosis. N ≥ 2 per condition.

(**B**) Cells were treated with aphidicolin and G2 phase duration (min) plotted according to Chk1 activity profile observed during G2.

(**A-B**) Lines are mean and 95% confidence interval. t test: *** $p < 0.001$, ** $p < 0.01$

(**C**) Cells were treated with aphidicolin in S phase then with DMSO or Chk1i in G2. 1/FRET values are normalized to G2 onset. Color code as in Fig. 2D. N>3

(**D**) Plotted cells were treated with aphidicolin in S phase then with DMSO, Chk1i or ATRi in G2 as in (C). Time interval from inhibitor addition in G2 to NEBD is plotted. Red lines: mean + standard Deviation. t test: *** $p < 0.001$. N>3

(**E**) Cells were treated with aphidicolin at t_{3h}. Each row represents a single cell. Color code of Chk1 activity profiles in G2 as in Fig. 4E. Re-entry into S phase during the second cell cycle is displayed in orange. N=3

(**F**) Cells were treated for 24h with CT, p53 or p21 siRNA then recorded for 48h. Aphidicolin was added at t_0 and cells plotted as in (E).

Star Methods

Resource availability

Lead contact

Further information and requests for resources and reagents should be directed to and will be fulfilled by the lead contact, Olivier Gavet (Olivier.gavet@gustaveroussy.fr).

Materials availability

All reagents generated in this study are available on request from the lead contact.

Data and code availability

. All data reported in this paper will be shared by the lead contact upon request.

. All original code has been deposited on Zenodo and is publicly available as of the date of publication. DOIs are listed in the key resources table.

. Any additional information required to reanalyze the data reported in this paper is available from the lead contact upon request.

EXPERIMENTAL MODEL AND SUBJECT DETAILS

Cell culture

Female hTert-RPE1 WT (ATCC; RRID:CVCL_4388), RPE1 mRuby-PCNA/+ and RPE1 mRuby-PCNA/+ Plk1-mVenus/+ cells , a gift from J. Mansfeld's laboratory, and their derivatives were cultured in DMEM/F12 medium (11320-039; Gibco) supplemented with 10% FCS (Eurobio Scientific), 100U/ml penicillin and 100µg/ml streptomycin (Gibco) at 37°C with 5% C02. Female HeLa and U20S (ATCC) cells were maintained in DMEM high glucose medium (Gibco; 41965-039), supplemented with 10% FCS and antibiotics.

HeLa cells were cultured in advanced DME (Invitrogen) supplemented with 2% FBS (Invitrogen), 200 µM Glutamax-1, 100 U/ml penicillin, 100 µg/ml streptomycin, and 250 ng/ml fungizone at 37°C with 10% CO2. For

METHOD DETAILS

Reagents

Chemical compounds dissolved in DMSO were used at the following concentrations unless stated otherwise: ATMi (KU55933 10µM), Cdc7i (XL-413 15µM), ATRi (AZD6738 1µM), Chk2i (PV1019 5µM or 25µM), Nutlin-3a (10µM), Cdk1/2 inhibitor III (600nM), Cdk1i (RO3306 10µM), Cdk2i (CVT-313 5µM), PolAi (ST1926 0.25µM), Plk1i (BI2536 150nM), Rad51i (B02 20µM), Rad52i (AICAR 20µM), PARPi (Olaparib 5µM), Etoposide 5µM, Hydroxyurea 1mM, Thymidine 1mM and Aphidicolin from 0.03 to 2µM. Unless stated otherwise, Chk1 inhibitor used was CHIR-124 (200nM). Other Chk1 inhibitors used were MK8776 (100nM) and LY2603618 (100nM).

Plasmid constructs

To generate a FRET-based Chk1 phosphorylation sensor, PCR amplification of the coding sequences for YPet (Nguyen et al. 2005) (NheI/AgeI), FHA2 domain (residues 572-730) from ScRad53 (NM_001183967) (AgeI/BamHI) and mTurquoise2 (Goedhart et al. 2012) tagged with SV40 NLS (amino acid sequence SPKKKRKVE) (EcoRI/EcoRV) were cloned by restriction digestion in that order on a pIRES-puro2 vector backbone (Clontech). Coding sequences for YPet and FHA2 domain originate from (Gheghiani et al., 2017), while mTurquoise2 sequence originates from a mTurquoise2-N1 plasmid (Addgene, #54843). To develop a specific Chk1 versus Chk2 FRET-based phosphorylation sensor, we tested different phosphorylation sequences inserted between the FHA2 domain and mTurquoise2 (BamHI/EcoRI) for which a preferential phosphorylation by Chk1 versus Chk2, at least *in vitro,* has been observed, such as Cdc25 T507 (Chen et al., 2003) or FANC-E (Kim et al., 2007), and a 6AA-Thr-6AA sequence containing key characteristics of the Chk1 consensus sequence (in bold): K-**L-R-R-**H-P-T-**F-**E-I-P-

L-A (Blasius et al., 2011). An isoleucine was always inserted at +3 position of the phosphorylated residue (underlined) for FHA2 binding (Durocher et al., 2000). The Chk1 sensor selected in the present work is made by the latter sequence. Overall structure: YPet (residues 1-239) - FHA2 residues (572-730) - K-L-R-R-H-P-T-F-E-I-P-L-A - mTurquoise2 (residues 1-239)-NLS. To generate chromatin targeted H2B-Chk1 sensor, H2B coding sequence was inserted upstream of YPet (NheI/NheI) in the pIRES-puro2 backbone.

Stable cell lines

To generate hTert-RPE1 WT or RPE1 mRuby-PCNA/+ cell lines stably expressing Chk1 phosphorylation sensor or its derivatives, 10^6 cells were electroporated with plasmid constructs using an Amaxa Nucleofector II device (Lonza, program X-001). Transfected cells were selected 48h later with puromycin or alternatively YFP and CFP double positives cells were first sorted on a BD FACS Aria III (BD Bioscience) before drug selection. After a minimum of two weeks of selection, isolated clones were picked up and amplified before characterization.

To generate U2OS cells stably expressing Chk1 sensor, transfection was performed with Jet PRIME reagent (Polyplus Transfection) according to the manufacturer's instructions, before selection of isolated clones as described above. For transient expression assays in HeLa cells (**Figure S1**), cells were seeded on 8-well glass bottom plates (µ–Dish, IBIDI) on J-2 and transfected using Jet PRIME reagent (Polyplus Transfection) the day before imaging.

Time-lapse imaging

RPE1 Cells were seeded at least 24h prior to imaging in phenol red-free DMEM/F12 medium (Gibco), supplemented with 5% FCS, 100U/ml penicillin and 100µg/ml streptomycin, in either 8-well glass-bottom plates (µ–Dish, IBIDI) or in 35mm glass-bottom dishes (Fluorodish, World Precision Instruments), both pre-coated with bovine fibronectin (C43050, PromoCell) at 1ug/cm2. HeLa and U2OS cells were seeded in DMEM without phenol red, supplemented with 5% FCS and antibiotics. For all experiments (except on Fig. S3B), live imaging was performed using an Eclipse Ti-e inverted microscope (Nikon) controlled by Metamorph software

(Molecular devices) and equipped with Perfect Focus System, fast emission filter wheel (lambda 10-3, Sutter Instruments), EMCCD camera (iXon Ultra 888, Andor) and LED-based illumination system (Spectra X-light engine, Lumencor). A Plan Fluor 40x/NA 1.30 oil immersion lens was used for all experiments, except on Fig 1D, S2E and S2F which were performed using a higher magnification 60x/NA 1.4 Plan Apochromat oil immersion lens. For FRET imaging assays, filters used (Chroma Technology) were ET434/21x excitation filter, 69008bs dichroic mirror, ET470/24m and ET535/30m emission filters for CFP and YFP channels, respectively. For mRuby-PCNA imaging, filters used were ET550/15x excitation filter, T565lp dichroic mirror and ET600/50m emission filter. During recordings, cells were maintained at 37°C in a humidified atmosphere with 5% CO2. Time-lapse on Fig. S3B was acquired on a Spinning Disk microscope based on a Yokogawa CSU-W1 confocal scanner unit mounted on a Nikon Eclipse Ti-2 inverted microscope equipped with a sCMOS PRIME 95B camera (Photometrics) and piloted by Metamorph Software. Excitation of CFP (FRET) and mRuby (PCNA) were respectively performed with a 445nm and 515nm laser source.

For phase contrast imaging assays, RPE1 cells were seeded on 12-well tissue culture plates in DMEM/F12 medium without phenol red, supplemented with 10% FBS and antibiotics, and then recorded 24h later. For analyses of the kinetics of mitotic entry, cells were recorded by phase-contrast video-microscopy and entry into mitosis for each cell was defined at NEBD.

Immunofluorescence

For **Figure S6K**, cells were seeded on fibronectin-coated glass-bottom µ-Dish 35mm Grid-50 (IBIDI), treated with 0.3 µM aphidicolin and filmed for 20h before fixation for 10min with 4% PFA. Cells were washed three times in PBS and then blocked 45 min in PBS+BSA 3%. Cells were incubated one hour with primary antibody in PBS + BSA 3%, washed three times in PBS + 0.1% Tween-20 (PBST) and incubated one hour with AlexaFluor 647 secondary antibody (Invitrogen). Cells were washed three times in PBST and then mounted with ProLong Gold AntiFade reagent with DAPI (Invitrogen). Gridded pattern was used to identify identical cells between film and

immunofluorescence by custom scripts written for Fiji. Time-lapse recording was used to determine Chk1 re-activation profile in G2 phase of each dividing cell and to identify daughter cells in G1 phase at the time of fixation. Immunofluorescence was used to count 53BP1 nuclear bodies in those G1 daughter cells.

siRNA transfection assays

For RNAi time-lapse assays, RPE1 cells were seeded in 35 mm glass-bottom dishes (Fluorodish, World Precision Instruments) or in 8-well glass-bottom plates (µ–Dish, IBIDI), respectively. Cells were transfected with siRNA (30nM final) using Dharmafect-1 reagent (Horizon Discovery) according to manufacturer's instructions. Live imaging assays were proceeded 24h or 48h later.

Western blotting

Cells were lysed in RIPA buffer (20mM Tris-HCl pH 7.5, 150mM NaCl, 10% Glycerol, 1% Triton X-100, 0.1% SDS, 1% Sodium deoxycholate with EDTA-free protease and phosphatase inhibitors (A32961, Thermo scientific). Protein quantification was performed in triplicate using BCA Protein Assay Kit (Thermofisher). Protein samples were separated on 4-15% Mini-Protean TGX precast gels (Bio-Rad). Western Blot images (16-bit) were acquired using an Amersham imager 600 (GE Healthcare) and quantified using ImageJ software (NIH).

Segmentation and tracking of cell nuclei

Nuclei segmentation, nuclei tracking and pixel measurements were performed in Fiji using custom scripts.

Segmentation: Cell nuclei were segmented using CFP excitation/YFP emission images from NLS-tagged Chk1 sensor. After Gaussian blur filtering and rolling-ball background subtraction to smooth background noise, a Mexican-hat filter was applied to enhance individual object boundaries. Resulting images were thresholded based on fluorescence intensity to isolate nuclei,

and further processed with a distance-based watershed to allow splitting of under-segmented nuclei.

Frame to frame nuclei matching: Nuclei detected in frame *n* were matched with the ones detected in frame *n+1* using a custom implementation of a Gale-Shapley algorithm for Fiji. Briefly,

1- For each objects (nuclei) in frame *n*, are listed all potential matches in frame *n+1*, ranked to maximize overlap area and/or minimize distance.
2- For each objects in frame *n+1*, are listed all potential matches in frame *n*, ranked to maximize overlap area and/or minimize distance.
3- Ranked preference lists are used to optimize matching of objects from frame *n* with objects with frame *n+1* (Gale-Shapley algorithm).

Any remaining non-matched objects in frame *n+1* are then used to identify potential over-segmentation and/or cytokinesis events by comparing between *n* and *n+1* frames distance and area of objects involved in putative splitting events. If an over-segmentation is indeed detected in frame *n+1*, objects in frame *n+1* are fused together. Conversely, any non-matched objects in frame *n* could reflect the under-segmentation of nuclei in frame *n+1*. This possibility is assessed by comparing between the two successive frames areas of all objects involved in the putative fusion event. If confirmed, detection of under-segmentation results in the automated splitting of the under-segmented nuclei in frame *n+1* using marker-controlled watershed. This approach allows to automatically segment and track next to all nuclei during long-term live imaging assays of high-density populations.

Measure pixel intensities: Following segmentation and tracking of individual nuclei, original raw images were processed with a carefully adjusted Rolling Ball background subtraction algorithm and pixel intensities were measured over time for all detected nuclei. All resulting data are saved in tables that can be further processed using custom python panda's scripts.

Determination of cell cycle phases

Nuclear mRuby-PCNA mean and max intensity over time were used to automatically identify cell cycle transitions:

G1/S transition: Mean PCNA expression is minimal in G1 and starts to increase around S phase transition (Zerjatke et al., 2017). To identify this inflexion point, we used a broken-stick approach by comparing slopes before and after all time points. To this end, for each time point, a local linear regression was calculated using all measurements 2.5 h before and another one using all measurements 2.5 h after. G1/S transition was determined as the time point that minimizes the calculated angle between the two linear regressions.

S/G2 transition: at the end of S phase, PCNA forms broad and very bright foci that disappear at G2 onset. This transition can be detected by extreme variations in the measured max mRuby-PCNA intensity in the nucleus. Two different algorithms were used: for asynchronous untreated cells, G2 onset was defined as the first local minimum following the highest measured peak in mRuby-PCNA max intensity in S phase. For cells treated with aphidicolin, a broken-stick approach was used to detect the inflexion point, as described above.

NEBD: At mitosis, the nuclear envelope is disassembled and soluble nuclear proteins are diluted in the whole volume of the cell. By measuring mRuby-PCNA signal over time, this is easily detectable by a sudden drop of mean intensity. Hence, mean mRuby-PCNA intensity was compared between all successive time points, and NEBD was defined as the time point when the maximal mean intensity drop occurred.

Automated classifications were systematically double-checked. An interface in Fiji was developed to manually review each cell and check for consistency between automatically determined cell cycle transitions and foci appearance/disappearance observed by eyes.

Classification of G2 phase Chk1 activity profiles

Classification of G2 Chk1 activity profiles was performed manually using the same interface, this time to systematically plot and review FRET variations during G2. Cells exhibiting no FRET increase up to NEBD were classified as "no Chk1 reactivation", cells exhibiting FRET increase

then decrease during G2 phase were classified as "transient Chk1 reactivation", and cells exhibiting FRET increase during G2 not followed by any significant decrease up to NEBD were classified as "persistent Chk1 reactivation".

Automated PCNA foci counting

To automatically count nuclear PCNA foci over time, images were processed with a Laplacian of Gaussian filter followed by local maxima detection to identify PCNA foci.

Data visualization

Data were plotted using GraphPad Prism or with custom python scripts relying on pandas for data manipulation and matplotlib or seaborn for data visualization. All scripts are available on request. For all graphs displaying cells synchronized *in silico* to the G1/S or S/G2 transition, all cells that exhibited a G1/S or S/G2 transition during recording (from 24h to 48h) are displayed, unless cell exited the field of view within the hour following the G1/S or S/G2 transition, which notably precluded classification of the Chk1 profile in G2 phase.

Ratiometric FRET images were generated using Fiji software by pixel-wise division of CFP over YFP images. An image mask was computed from the segmented nuclei and all pixels outside were defined as 0 (black). Ratiometric images are displayed using Fiji *mpl inferno* Look-Up Table.

QUANTIFICATION AND STATISTICAL ANALYSIS

Column data of Figure 3C, 6A, 6B, 6D, S2G, S2H, S6H was compared pairwise using a t-test. Further statistical details of the experiment can be found in figure legends. Unless otherwise stated in the legend, center of column data is defined as the mean value and the error bars stand for the standard deviation. For the box plots, the box ends are the quartiles, the horizontal line inside the box is the median, and the whiskers extend out to the farthest points that are not outliers. For figure 6E-F, proportions of cells re-entering S phase were compared with a Chi

Square test with one degree of freedom, as indicated on the figure. For all figures displaying cells synchronized *in silico* to the G1/S or S/G2 transition, all cells that exhibited a G1/S or S/G2 transition during recording are displayed, unless a cell exited the field of view within the hour following the G1/S or S/G2 transition, which notably precluded the classification of the G2 phase Chk1 profile. No other exclusion criterion was used. Data was not randomized prior to analysis. For all data except Figure 4D, 5B and S6F, figure displays the results of a representative experiment. For all figures, n is the number of cells in displayed experiment, and N the number of replicate experiments. All statistical analysis was performed in Graphpad Prism and resulting p values are either indicated on graph, or stated as an interval on the graph or in the legends (e.g.: $p < 0.001$). Significance is defined as $p < 0.05$.

Bibliography

Ait Saada, A., Lambert, S.A.E., and Carr, A.M. (2018). Preserving replication fork integrity and competence via the homologous recombination pathway. DNA Repair (Amst). *71*, 135–147.

Akopyan, K., SilvaCascales, H., Hukasova, E., Saurin, A.T., Müllers, E., Jaiswal, H., Hollman, D.A.A., Kops, G.J.P.L., Medema, R., and Lindqvist, A. (2014). Assessing kinetics from fixed cells reveals activation of the mitotic entry network at the S/G2 transition. Mol. Cell *53*, 843–853.

Alver, R.C., Chadha, G.S., Gillespie, P.J., and Blow, J.J. (2017). Reversal of DDK-Mediated MCM Phosphorylation by Rif1-PP1 Regulates Replication Initiation and Replisome Stability Independently of ATR/Chk1. Cell Rep. *18*, 2508–2520.

Barr, A.R., Cooper, S., Heldt, F.S., Butera, F., Stoy, H., Mansfeld, J., Novák, B., and Bakal, C. (2017). DNA damage during S-phase mediates the proliferation-quiescence decision in the subsequent G1 via p21 expression. Nat. Commun. *8*.

Bartek, J., and Lukas, J. (2007). DNA damage checkpoints: from initiation to recovery or adaptation. Curr. Opin. Cell Biol. *19*, 238–245.

Bartkova, J., Hořejší, Z., Koed, K., Krämer, A., Tort, F., Zleger, K., Guldberg, P., Sehested, M., Nesland, J.M., Lukas, C., et al. (2005). DNA damage response as a candidate anti-cancer barrier in early human tumorigenesis. Nature *434*, 864–870.

Bass, T.E., Luzwick, J.W., Kavanaugh, G., Carroll, C., Dungrawala, H., Glick, G.G., Feldkamp, M.D., Putney, R., Chazin, W.J., and Cortez, D. (2016). ETAA1 acts at stalled replication forks to maintain genome integrity. Nat. Cell Biol. *18*, 1185–1195.

Blasius, M., Forment, J. V., Thakkar, N., Wagner, S.A., Choudhary, C., and Jackson, S.P. (2011). A phospho-proteomic screen identifies substrates of the checkpoint kinase Chk1. Genome Biol. *12*, 1–14.

Buisson, R., Boisvert, J.L., Benes, C.H., and Zou, L. (2015). Distinct but Concerted Roles of ATR, DNA-PK, and Chk1 in Countering Replication Stress during S Phase. Mol. Cell *59*, 1011–1024.

Bunz, F., Dutriaux, A., Lengauer, C., Waldman, T., Zhou, S., Brown, J.P., Sedivy, J.M., Kinzler, K.W., and Vogelstein, B. (1998). Requirement for p53 and p21 to sustain G2 arrest after DNA damage. Science (80-.). *282*, 1497–1501.

Burrell, R.A., McClelland, S.E., Endesfelder, D., Groth, P., Weller, M.C., Shaikh, N., Domingo, E., Kanu, N., Dewhurst, S.M., Gronroos, E., et al. (2013). Replication stress links structural and numerical cancer chromosomal instability. Nature *494*, 492–496.

Chagin, V.O., Casas-Delucchi, C.S., Reinhart, M., Schermelleh, L., Markaki, Y., Maiser, A., Bolius, J.J., Bensimon, A., Fillies, M., Domaing, P., et al. (2016). 4D Visualization of replication foci in mammalian cells corresponding to individual replicons. Nat. Commun. *7*, 1–12.

Chen, M.-S., Ryan, C.E., and Piwnica-Worms, H. (2003). Chk1 Kinase Negatively Regulates

Mitotic Function of Cdc25A Phosphatase through 14-3-3 Binding. Mol. Cell. Biol. *23*, 7488–7497.

Ciardo, D., Goldar, A., and Marheineke, K. (2019). On the interplay of the DNA replication program and the Intra-S phase checkpoint pathway. Genes (Basel). *10*.

Courbet, S., Gay, S., Arnoult, N., Wronka, G., Anglana, M., Brison, O., and Debatisse, M. (2008). Replication fork movement sets chromatin loop size and origin choice in mammalian cells. Nature *455*, 557–560.

Daigh, L.H., Liu, C., Chung, M., Cimprich, K.A., and Meyer, T. (2018). Stochastic Endogenous Replication Stress Causes ATR-Triggered Fluctuations in CDK2 Activity that Dynamically Adjust Global DNA Synthesis Rates. Cell Syst. *7*, 17–27.

Debatisse, M., and Rosselli, F. (2019). A journey with common fragile sites: From S phase to telophase. Genes Chromosom. Cancer *58*, 305–316.

Durocher, D., Taylor, I.A., Sarbassova, D., Haire, L.F., Westcott, S.L., Jackson, S.P., Smerdon, S.J., and Yaffe, M.B. (2000). The molecular basis of FHA domain: Phosphopeptide binding specificity and implications for phospho-dependent signaling mechanisms. Mol. Cell *6*, 1169–1182.

Duursma, A.M., Driscoll, R., Elias, J.E., and Cimprich, K.A. (2013). A Role for the MRN Complex in ATR Activation via TOPBP1 Recruitment. Mol. Cell *50*, 116–122.

Ercilla, A., Benada, J., Amitash, S., Zonderland, G., Baldi, G., Somyajit, K., Ochs, F., Costanzo, V., Lukas, J., and Toledo, L. (2020). Physiological Tolerance to ssDNA Enables Strand Uncoupling during DNA Replication. Cell Rep. *30*, 2416–2429.

Eykelenboom, J.K., Harte, E.C., Canavan, L., Pastor-Peidro, A., Calvo-Asensio, I., Llorens-Agost, M., and Lowndes, N.F. (2013). ATR Activates the S-M Checkpoint during Unperturbed Growth to Ensure Sufficient Replication Prior to Mitotic Onset. Cell Rep. *5*, 1095–1107.

Forey, R., Poveda, A., Sharma, S., Barthe, A., Padioleau, I., Renard, C., Lambert, R., Skrzypczak, M., Ginalski, K., Lengronne, A., et al. (2020). Mec1 Is Activated at the Onset of Normal S Phase by Low-dNTP Pools Impeding DNA Replication. Mol. Cell *78*, 396–410.

Gavet, O., and Pines, J. (2010). Progressive Activation of CyclinB1-Cdk1 Coordinates Entry to Mitosis. Dev. Cell *18*, 533–543.

Gheghiani, L., and Gavet, O. (2016). Spatiotemporal investigation of phosphorylation events during cell cycle progression. Methods Mol. Biol. *1342*, 157–171.

Gheghiani, L., Loew, D., Lombard, B., Mansfeld, J., and Gavet, O. (2017). PLK1 Activation in Late G2 Sets Up Commitment to Mitosis. Cell Rep. *19*, 2060–2073.

Goldstone, S., Pavey, S., Forrest, A., Sinnamon, J., and Gabrielli, B. (2001). Cdc25-dependent activation of cyclin A/cdk2 is blocked in G2 phase arrested cells independently of ATM/ATR. Oncogene *20*, 921–932.

Gong, D., Pomerening, J.R., Myers, J.W., Gustavsson, C., Jones, J.T., Hahn, A.T., Meyer, T., and Ferrell, J.E. (2007). Cyclin A2 Regulates Nuclear-Envelope Breakdown and the

Nuclear Accumulation of Cyclin B1. Curr. Biol. *17*, 85–91.

Goto, H., Natsume, T., Kanemaki, M.T., Kaito, A., Wang, S., Gabazza, E.C., Inagaki, M., and Mizoguchi, A. (2019). Chk1-mediated Cdc25A degradation as a critical mechanism for normal cell cycle progression. J. Cell Sci. *132*.

Haahr, P., Hoffmann, S., Tollenaere, M.A.X., Ho, T., Toledo, L.I., Mann, M., Bekker-Jensen, S., Räschle, M., and Mailand, N. (2016). Activation of the ATR kinase by the RPA-binding protein ETAA1. Nat. Cell Biol. *18*, 1196–1207.

Hastak, K., Paul, R.K., Agarwal, M.K., Thakur, V.S., Amin, A.R.M.R., Agrawal, S., Sramkoski, R.M., Jacobberger, J.W., Jackson, M.W., Stark, G.R., et al. (2008). DNA synthesis from unbalanced nucleotide pools causes limited DNA damage that triggers ATR-CHK1-dependent p53 activation. Proc. Natl. Acad. Sci. U. S. A. *105*, 6314–6319.

Hégarat, N., Crncec, A., Suarez Peredo Rodriguez, M.F., Echegaray Iturra, F., Gu, Y., Busby, O., Lang, P.F., Barr, A.R., Bakal, C., Kanemaki, M.T., et al. (2020). Cyclin A triggers Mitosis either via the Greatwall kinase pathway or Cyclin B. EMBO J. *39*, 1–23.

Hills, S.A., and Diffley, J.F.X. (2014). DNA replication and oncogene-induced replicative stress. Curr. Biol. *24*, R435–R444.

Huang, F., Mazina, O.M., Zentner, I.J., Cocklin, S., and Mazin, A. V. (2012). Inhibition of homologous recombination in human cells by targeting RAD51 recombinase. J. Med. Chem. *55*, 3011–3020.

Huertas, P., and Jackson, S.P. (2009). Human CtIP mediates cell cycle control of DNA end resection and double strand break repair. J. Biol. Chem. *284*, 9558–9565.

Jazayeri, A., Falck, J., Lukas, C., Bartek, J., Smith, G.C.M., Lukas, J., and Jackson, S.P. (2006). ATM- and cell cycle-dependent regulation of ATR in response to DNA double-strand breaks. Nat. Cell Biol. *8*, 37–45.

Kalsbeek, D., and Golsteyn, R.M. (2017). G2/M-phase checkpoint adaptation and micronuclei formation as mechanisms that contribute to genomic instability in human cells. Int. J. Mol. Sci. *18*.

Kim, M.A., Kim, H.J., Brown, A.L., Lee, M.Y., Bae, Y.S., Park, J.I., Kwak, J.Y., Chung, J.H., and Yun, J. (2007). Identification of novel substrates for human checkpoint kinase Chk1 and Chk2 through genome-wide screening using a consensus Chk phosphorylation motif. Exp. Mol. Med. *39*, 205–212.

Koundrioukoff, S., Carignon, S., Técher, H., Letessier, A., Brison, O., and Debatisse, M. (2013). Stepwise Activation of the ATR Signaling Pathway upon Increasing Replication Stress Impacts Fragile Site Integrity. PLoS Genet. *9*.

Krenning, L., Feringa, F.M., Shaltiel, I.A., vandenBerg, J., and Medema, R.H. (2014). Transient activation of p53 in G2 phase is sufficient to induce senescence. Mol. Cell *55*, 59–72.

Laoukili, J., Alvarez, M., Meijer, L.A.T., Stahl, M., Mohammed, S., Kleij, L., Heck, A.J.R., and Medema, R.H. (2008). Activation of FoxM1 during G 2 Requires Cyclin A/Cdk-Dependent Relief of Autorepression by the FoxM1 N-Terminal Domain . Mol. Cell. Biol. *28*, 3076–

3087.

Lee, Y.C., Zhou, Q., Chen, J., and Yuan, J. (2016). RPA-Binding Protein ETAA1 Is an ATR Activator Involved in DNA Replication Stress Response. Curr. Biol. *26*, 3257–3268.

Lemmens, B., and Lindqvist, A. (2019). DNA replication and mitotic entry: A brake model for cell cycle progression. J. Cell Biol. *218*, 3892–3902.

Lemmens, B., Hegarat, N., Akopyan, K., Sala-Gaston, J., Bartek, J., Hochegger, H., and Lindqvist, A. (2018). DNA Replication Determines Timing of Mitosis by Restricting CDK1 and PLK1 Activation. Mol. Cell *71*, 117–128.

Leonhardt, H., Rahn, H.P., Weinzierl, P., Sporbert, A., Cremer, T., Zink, D., and Cardoso, M.C. (2000). Dynamics of DNA replication factories in living cells. J. Cell Biol. *149*, 271–279.

Lim, G., Chang, Y., and Huh, W.K. (2020). Phosphoregulation of Rad51/Rad52 by CDK1 functions as a molecular switch for cell cycle–specific activation of homologous recombination. Sci. Adv. *6*.

Lopes, M., Foiani, M., and Sogo, J.M. (2006). Multiple mechanisms control chromosome integrity after replication fork uncoupling and restart at irreparable UV lesions. Mol. Cell *21*, 15–27.

Macůrek, L., Lindqvist, A., Lim, D., Lampson, M.A., Klompmaker, R., Freire, R., Clouin, C., Taylor, S.S., Yaffe, M.B., and Medema, R.H. (2008). Polo-like kinase-1 is activated by aurora A to promote checkpoint recovery. Nature *455*, 119–123.

Maya-Mendoza, A., Petermann, E., Gillespie, D.A.F., Caldecott, K.W., and Jackson, D.A. (2007). Chk1 regulates the density of active replication origins during the vertebrate S phase. EMBO J. *26*, 2719–2731.

Merrick, K.A., Larochelle, S., Zhang, C., Allen, J.J., Shokat, K.M., and Fisher, R.P. (2008). Distinct Activation Pathways Confer Cyclin-Binding Specificity on Cdk1 and Cdk2 in Human Cells. Mol. Cell *32*, 662–672.

Minocherhomji, S., Ying, S., Bjerregaard, V.A., Bursomanno, S., Aleliunaite, A., Wu, W., Mankouri, H.W., Shen, H., Liu, Y., and Hickson, I.D. (2015). Replication stress activates DNA repair synthesis in mitosis. Nature *528*, 286–290.

Murphy, C.M., and Michael, W.M. (2013). Control of DNA replication by the nucleus/cytoplasm ratio in xenopus. J. Biol. Chem. *288*, 29382–29393.

Pagano, M., Pepperkok, R., Verde, F., Ansorge, W., and Draetta, G. (1992). Cyclin A is required at two points in the human cell cycle. EMBO J. *11*, 961–971.

Palermo, V., Rinalducci, S., Sanchez, M., Grillini, F., Sommers, J.A., Brosh, R.M., Zolla, L., Franchitto, A., and Pichierri, P. (2016). CDK1 phosphorylates WRN at collapsed replication forks. Nat. Commun. *7*.

Petermann, E., Woodcock, M., and Helleday, T. (2010a). Chk1 promotes replication fork progression by controlling replication initiation. Proc. Natl. Acad. Sci. U. S. A. *107*, 16090–16095.

Petermann, E., Orta, M.L., Issaeva, N., Schultz, N., and Helleday, T. (2010b). Hydroxyurea-Stalled Replication Forks Become Progressively Inactivated and Require Two Different RAD51-Mediated Pathways for Restart and Repair. Mol. Cell *37*, 492–502.

Saldivar, J.C., Hamperl, S., Bocek, M.J., Chung, M., Bass, T.E., Cisneros-Soberanis, F., Samejima, K., Xie, L., Paulson, J.R., Earnshaw, W.C., et al. (2018). An intrinsic S/G2 checkpoint enforced by ATR. Science (80-.). *361*, 806–810.

Sasi, N.K., Coquel, F., Lin, Y.L., MacKeigan, J.P., Pasero, P., and Weinreich, M. (2018). DDK Has a Primary Role in Processing Stalled Replication Forks to Initiate Downstream Checkpoint Signaling. Neoplasia (United States) *20*, 985–995.

Seki, A., Coppinger, J.A., Jang, C., Iii, J.R.Y., and Fang, G. (2008). Bora and the Kinase Activate Cooperatively Plkl and Control Mitotic the Kinase Entry. Science (80-.). *320*, 1655–1658.

Smits, V.A.J., Reaper, P.M., and Jackson, S.P. (2006). Rapid PIKK-dependent release of Chk1 from chromatin promotes the DNA-damage checkpoint response. Curr. Biol. *16*, 150–159.

Syljuåsen, R.G. (2007). Checkpoint adaptation in human cells. Oncogene *26*, 5833–5839.

Syljuåsen, R.G., Jensen, S., Bartek, J., and Lukas, J. (2006). Adaptation to the ionizing radiation-induced G2 checkpoint occurs in human cells and depends on checkpoint kinase 1 and polo-like kinase 1 kinases. Cancer Res. *66*, 10253–10257.

Tavernier, N., Thomas, Y., Vigneron, S., Maisonneuve, P., Orlicky, S., Mader, P., Regmi, S.G., Van Hove, L., Levinson, N.M., Gasmi-Seabrook, G., et al. (2021). Bora phosphorylation substitutes in trans for T-loop phosphorylation in Aurora A to promote mitotic entry. Nat. Commun. *12*, 1–22.

Técher, H., Koundrioukoff, S., Nicolas, A., and Debatisse, M. (2017). The impact of replication stress on replication dynamics and DNA damage in vertebrate cells. Nat. Rev. Genet. *18*, 535–550.

Tirman, S., Quinet, A., Wood, M., Meroni, A., Cybulla, E., Jackson, J., Pegoraro, S., Simoneau, A., Zou, L., and Vindigni, A. (2021). Temporally distinct post-replicative repair mechanisms fill PRIMPOL-dependent ssDNA gaps in human cells. Mol. Cell *81*, 4026-4040.e8.

Toczyski, D.P., Galgoczy, D.J., and Hartwell, L.H. (1997). CDC5 and CKII control adaptation to the yeast DNA damage checkpoint. Cell *90*, 1097–1106.

Tomimatsu, N., Mukherjee, B., Catherine Hardebeck, M., Ilcheva, M., Vanessa Camacho, C., Louise Harris, J., Porteus, M., Llorente, B., Khanna, K.K. u., and Burma, S. (2014). Phosphorylation of EXO1 by CDKs 1 and 2 regulates DNA end resection and repair pathway choice. Nat. Commun. *5*, 3561.

Trovesi, C., Manfrini, N., Falcettoni, M., and Longhese, M.P. (2013). Regulation of the DNA damage response by cyclin-dependent kinases. J. Mol. Biol. *425*, 4756–4766.

Tsantoulis, P.K., Kotsinas, A., Sfikakis, P.P., Evangelou, K., Sideridou, M., Levy, B., Mo, L., Kittas, C., Wu, X.R., Papavassiliou, A.G., et al. (2008). Oncogene-induced replication stress

preferentially targets common fragile sites in preneoplastic lesions. A genome-wide study. Oncogene *27*, 3256–3264.

Tse, A.N., Rendahl, K.G., Sheikh, T., Cheema, H., Aardalen, K., Embry, M., Ma, S., Moler, E.J., Zhi, J.N., De Menezes, D.E.L., et al. (2007). CHIR-124, a novel potent inhibitor of Chk1, potentiates the cytotoxicity of topoisomerase I poisons in vitro and in vivo. Clin. Cancer Res. *13*, 591–602.

Van, C., Yan, S., Michael, W.M., Waga, S., and Cimprich, K.A. (2010). Continued primer synthesis at stalled replication forks contributes to checkpoint activation. J. Cell Biol. *189*, 233–246.

Vassilev, L.T., Vu, B.T., Graves, B., Carvajal, D., Podlaski, F., Filipovic, Z., Kong, N., Kammlott, U., Lukacs, C., Klein, C., et al. (2004). In Vivo Activation of the p53 Pathway by Small-Molecule Antagonists of MDM2. Science (80-.). *303*, 844–848.

Vigneron, S., Sundermann, L., Labbé, J.C., Pintard, L., Radulescu, O., Castro, A., and Lorca, T. (2018). Cyclin A-cdk1-Dependent Phosphorylation of Bora Is the Triggering Factor Promoting Mitotic Entry. Dev. Cell *45*, 637-650.e7.

Watanabe, N., Arai, H., Iwasaki, J., Shiina, M., Ogata, K., Hunter, T., and Osada, H. (2005). Cyclin-dependent kinase (CDK) phosphorylation destabilizes somatic Wee1 via multiple pathways. Proc. Natl. Acad. Sci. U. S. A. *102*, 11663–11668.

Wilhelm, T., Olziersky, A.M., Harry, D., De Sousa, F., Vassal, H., Eskat, A., and Meraldi, P. (2019). Mild replication stress causes chromosome mis-segregation via premature centriole disengagement. Nat. Commun. *10*, 1–14.

Xu, Y., Ning, S., Wei, Z., Xu, R., Xu, X., Xing, M., Guo, R., and Xu, D. (2017). 53BP1 and BRCA1 control pathway choice for stalled replication restart. Elife *6*, 1–24.

Yamazaki, S., Ishii, A., Kanoh, Y., Oda, M., Nishito, Y., and Masai, H. (2012). Rif1 regulates the replication timing domains on the human genome. EMBO J. *31*, 3667–3677.

Yang, H.W., Chung, M., Kudo, T., and Meyer, T. (2017). Competing memories of mitogen and p53 signalling control cell-cycle entry. Nature *549*, 404–408.

Yata, K., and Esashi, F. (2009). Dual role of CDKs in DNA repair: To be, or not to be. DNA Repair (Amst). *8*, 6–18.

Yata, K., Lloyd, J., Maslen, S., Bleuyard, J.Y., Skehel, M., Smerdon, S.J., and Esashi, F. (2012). Plk1 and CK2 Act in Concert to Regulate Rad51 during DNA Double Strand Break Repair. Mol. Cell *45*, 371–383.

Yata, K., Bleuyard, J.Y., Nakato, R., Ralf, C., Katou, Y., Schwab, R.A., Niedzwiedz, W., Shirahige, K., and Esashi, F. (2014). BRCA2 coordinates the activities of cell-cycle kinases to promote genome stability. Cell Rep. *7*, 1547–1559.

Yoo, H.Y., Kumagai, A., Shevchenko, A., Shevchenko, A., and Dunphy, W.G. (2004). Adaptation of a DNA replication checkpoint response depends upon inactivation of Claspin by the Polo-like kinase. Cell *117*, 575–588.

Zellweger, R., Dalcher, D., Mutreja, K., Berti, M., Schmid, J.A., Herrador, R., Vindigni, A.,

and Lopes, M. (2015). Rad51-mediated replication fork reversal is a global response to genotoxic treatments in human cells. J. Cell Biol. *208*, 563–579.

Zerjatke, T., Gak, I.A., Kirova, D., Fuhrmann, M., Daniel, K., Gonciarz, M., Müller, D., Glauche, I., and Mansfeld, J. (2017). Quantitative Cell Cycle Analysis Based on an Endogenous All-in-One Reporter for Cell Tracking and Classification. Cell Rep. *19*, 1953–1966.

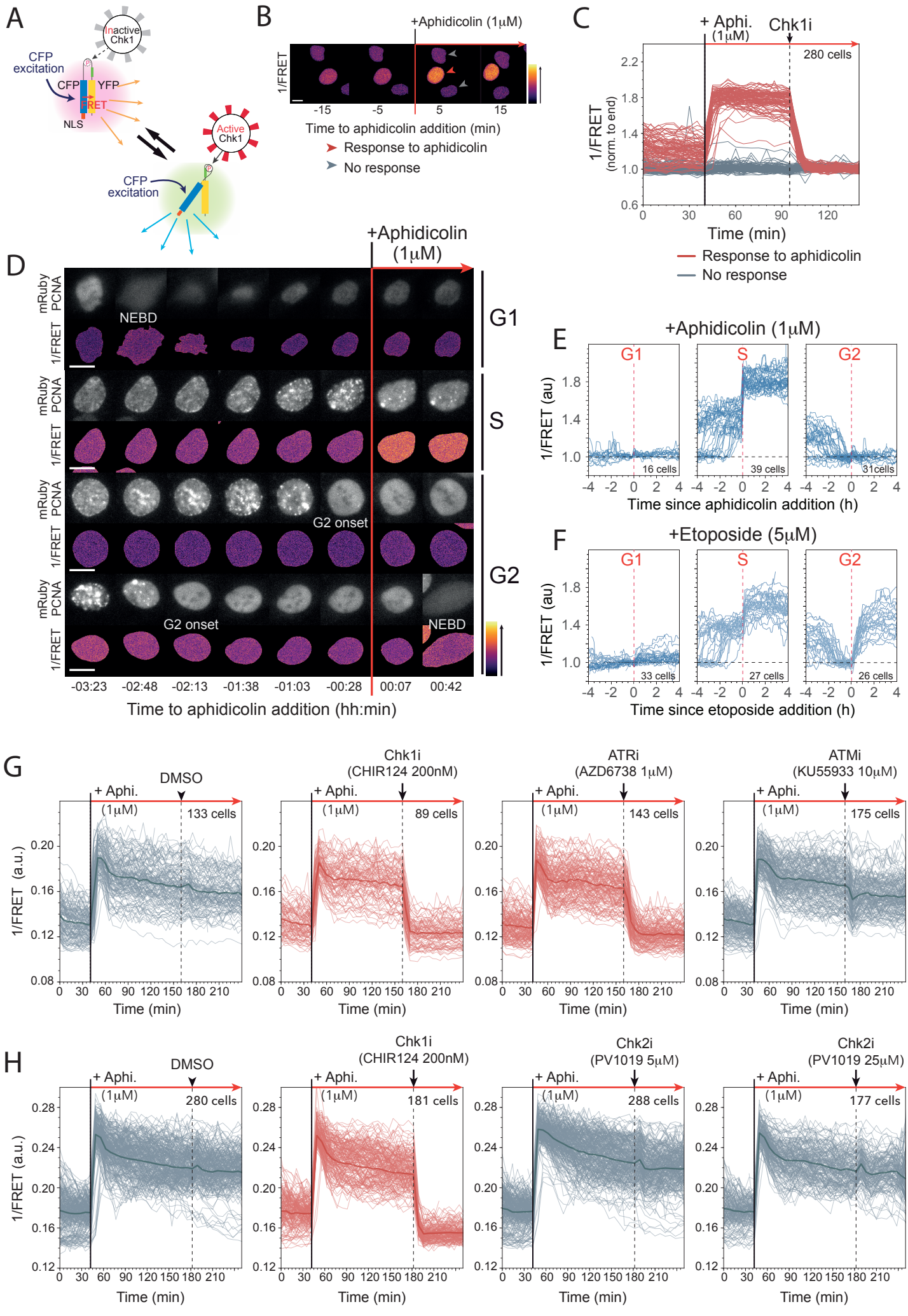
A
Inactive Chk1
CFP excitation
CFP
YFP
FRET
NLS
Active Chk1
CFP excitation
B
+Aphidicolin (1μM)
1/FRET
-15
-5
5
15
Time to aphidicolin addition (min)
Response to aphidicolin
No response
C
+ Aphi. (1μM)
Chk1i
280 cells
1/FRET (norm. to end)
Time (min)
Response to aphidicolin
No response
D
+Aphidicolin (1μM)
mRuby PCNA
1/FRET
NEBD
G2 onset
G2 onset
NEBD
G1
S
G2
-03:23
-02:48
-02:13
-01:38
-01:03
-00:28
00:07
00:42
Time to aphidicolin addition (hh:min)
E
+Aphidicolin (1μM)
G1
S
G2
1/FRET (au)
16 cells
39 cells
31cells
Time since aphidicolin addition (h)
F
+Etoposide (5μM)
G1
S
G2
1/FRET (au)
33 cells
27 cells
26 cells
Time since etoposide addition (h)
G
DMSO
Chk1i (CHIR124 200nM)
ATRi (AZD6738 1μM)
ATMi (KU55933 10μM)
+ Aphi. (1μM)
133 cells
89 cells
143 cells
175 cells
1/FRET (a.u.)
Time (min)
H
DMSO
Chk1i (CHIR124 200nM)
Chk2i (PV1019 5μM)
Chk2i (PV1019 25μM)
+ Aphi. (1μM)
280 cells
181 cells
288 cells
177 cells
1/FRET (a.u.)
Time (min)

FIGURE 1

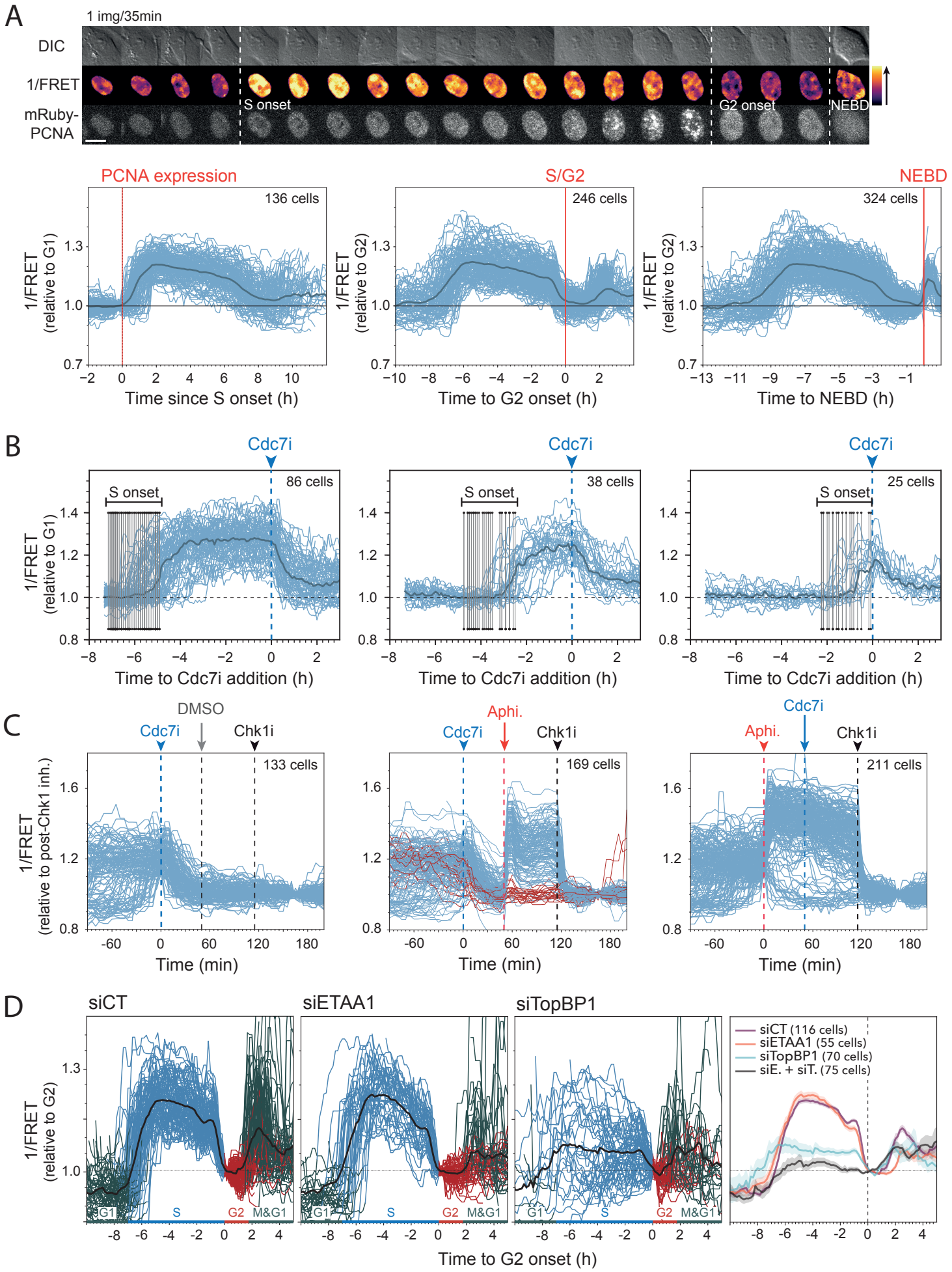
A
1 img/35min
DIC
1/FRET
mRuby-PCNA
S onset
G2 onset
NEBD
PCNA expression
S/G2
NEBD
136 cells
246 cells
324 cells
1/FRET (relative to G1)
1/FRET (relative to G2)
Time since S onset (h)
Time to G2 onset (h)
Time to NEBD (h)
B
Cdc7i
S onset
86 cells
38 cells
25 cells
Time to Cdc7i addition (h)
C
DMSO
Cdc7i
Chk1i
Aphi.
133 cells
169 cells
211 cells
1/FRET (relative to post-Chk1 inh.)
Time (min)
D
siCT
siETAA1
siTopBP1
G1
S
G2
M&G1
siCT (116 cells)
siETAA1 (55 cells)
siTopBP1 (70 cells)
siE. + siT. (75 cells)
Time to G2 onset (h)

FIGURE 2

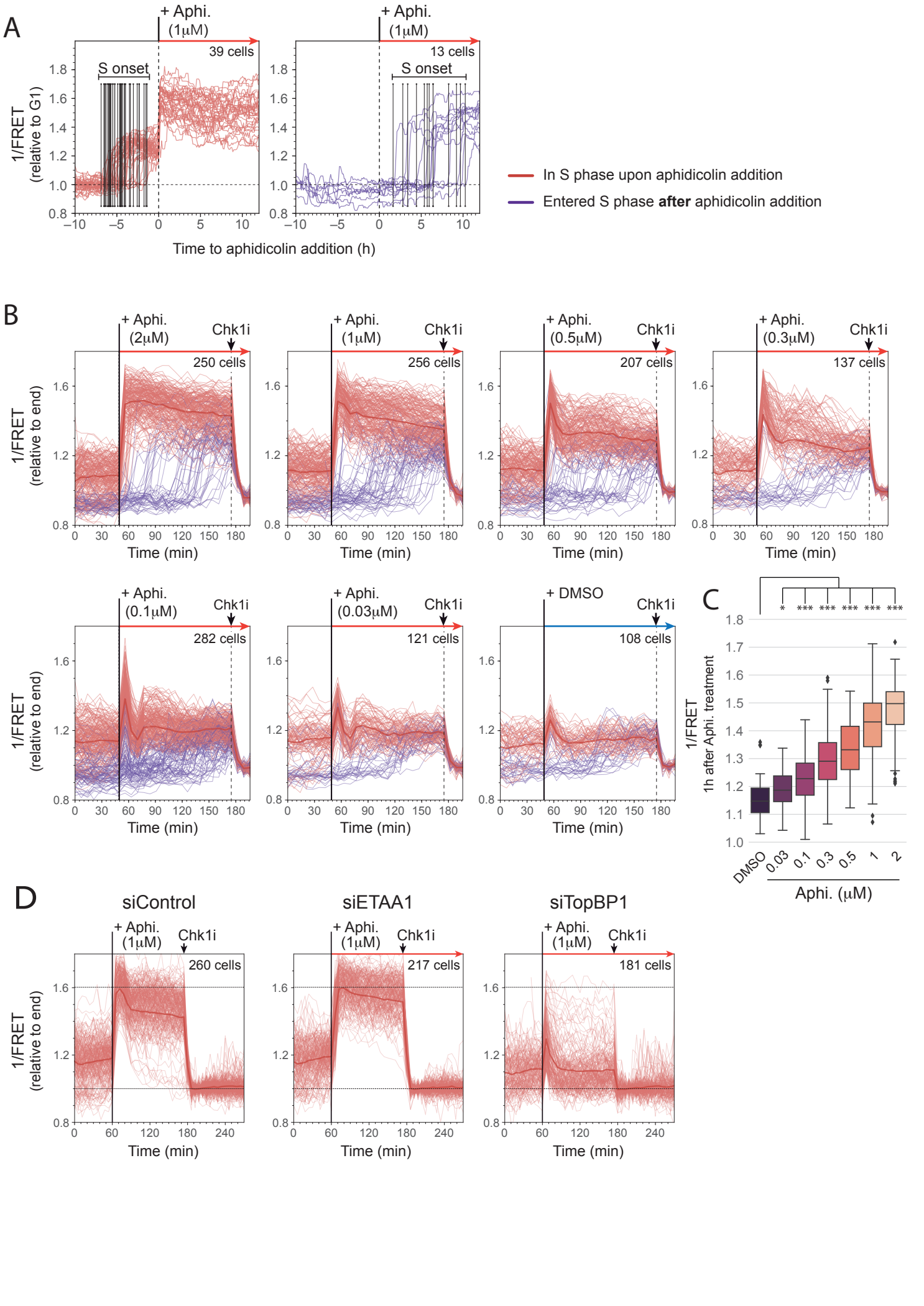
A
+ Aphi. (1μM)
39 cells
13 cells
S onset
1/FRET (relative to G1)
Time to aphidicolin addition (h)
In S phase upon aphidicolin addition
Entered S phase after aphidicolin addition
B
+ Aphi. (2μM)
+ Aphi. (1μM)
+ Aphi. (0.5μM)
+ Aphi. (0.3μM)
+ Aphi. (0.1μM)
+ Aphi. (0.03μM)
+ DMSO
Chk1i
250 cells
256 cells
207 cells
137 cells
282 cells
121 cells
108 cells
1/FRET (relative to end)
Time (min)
C
1/FRET 1h after Aphi. treatment
DMSO
0.03
0.1
0.3
0.5
1
2
Aphi. (μM)
D
siControl
siETAA1
siTopBP1
260 cells
217 cells
181 cells

FIGURE 3

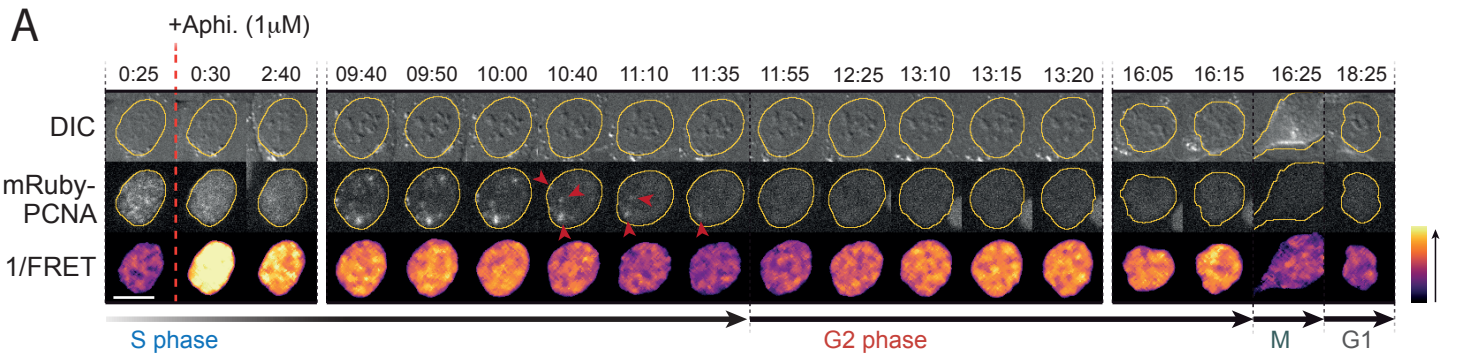
A
+Aphi. (1μM)
0:25
0:30
2:40
09:40
09:50
10:00
10:40
11:10
11:35
11:55
12:25
13:10
13:15
13:20
16:05
16:15
16:25
18:25
DIC
mRuby-PCNA
1/FRET
S phase
G2 phase
M
G1

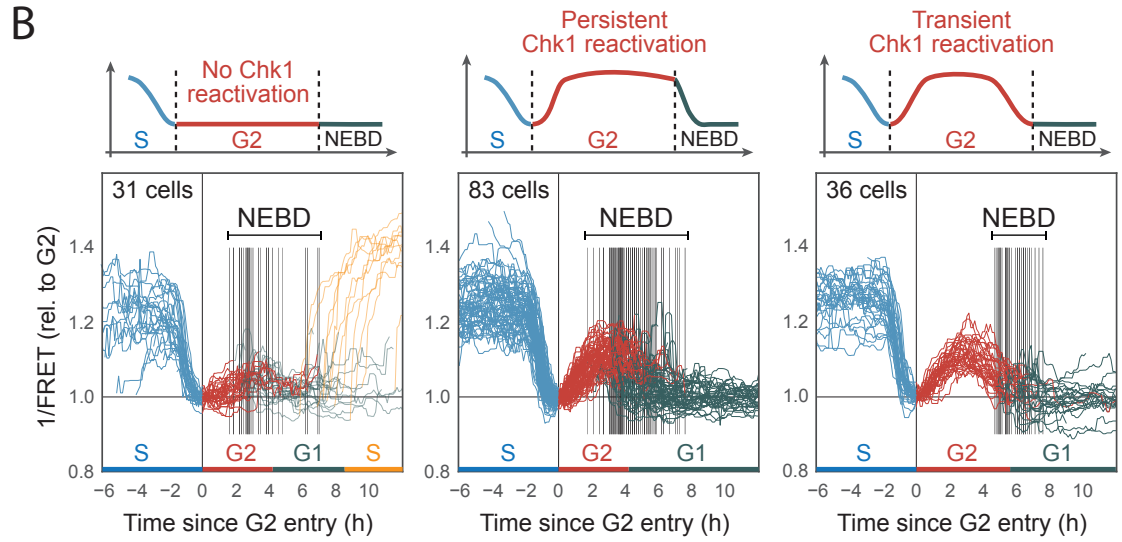
B
No Chk1 reactivation
Persistent Chk1 reactivation
Transient Chk1 reactivation
S
G2
NEBD
31 cells
83 cells
36 cells
1/FRET (rel. to G2)
Time since G2 entry (h)
G1

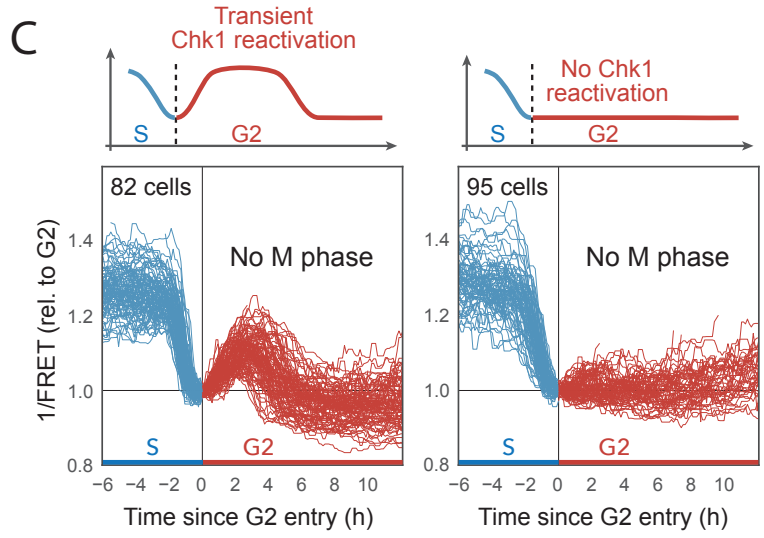
C
Transient Chk1 reactivation
No Chk1 reactivation
82 cells
95 cells
No M phase
1/FRET (rel. to G2)
Time since G2 entry (h)

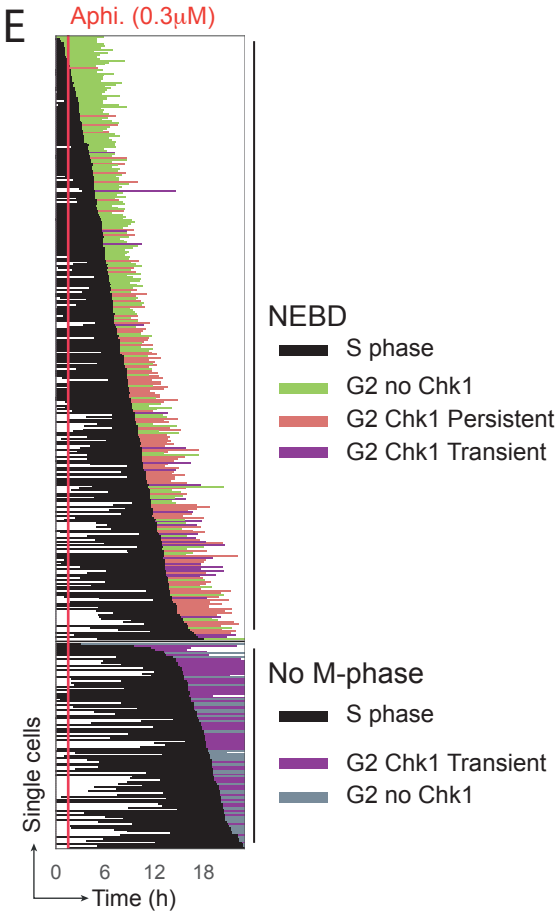
E
Aphi. (0.3μM)
NEBD
S phase
G2 no Chk1
G2 Chk1 Persistent
G2 Chk1 Transient
No M-phase
S phase
G2 Chk1 Transient
G2 no Chk1
Single cells
Time (h)

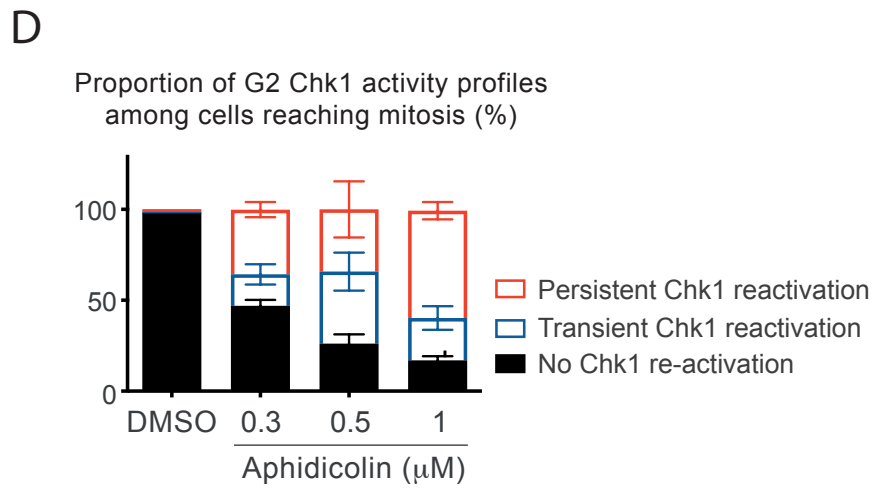
D
Proportion of G2 Chk1 activity profiles among cells reaching mitosis (%)
Persistent Chk1 reactivation
Transient Chk1 reactivation
No Chk1 re-activation
DMSO
0.3
0.5
1
Aphidicolin (μM)

FIGURE 4

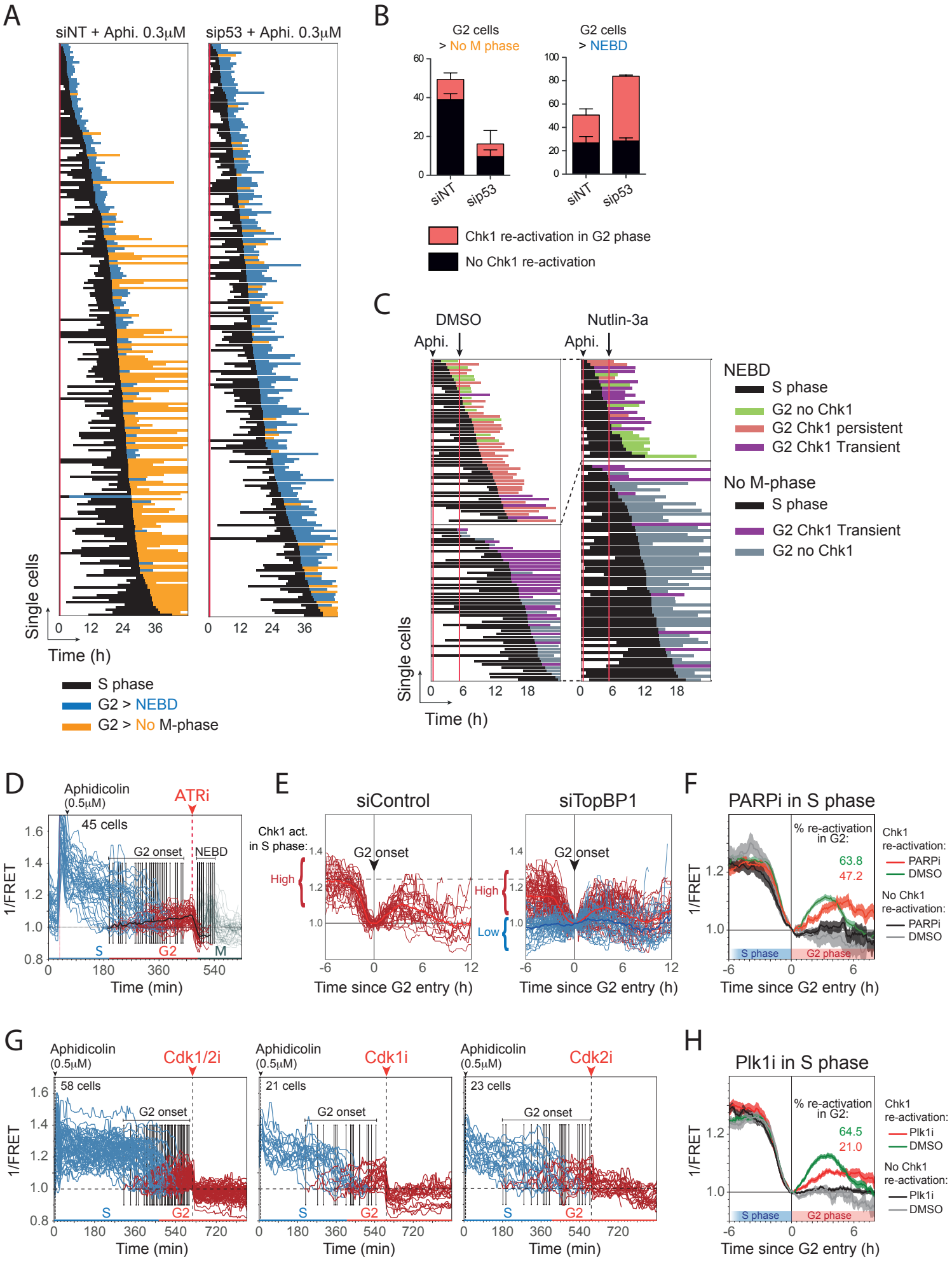
A
siNT + Aphi. 0.3μM
sip53 + Aphi. 0.3μM
Single cells
0 12 24 36
Time (h)
S phase
G2 > NEBD
G2 > No M-phase
B
G2 cells
> No M phase
G2 cells
> NEBD
siNT
sip53
Chk1 re-activation in G2 phase
No Chk1 re-activation
C
DMSO
Aphi.
Nutlin-3a
Aphi.
Single cells
Time (h)
NEBD
S phase
G2 no Chk1
G2 Chk1 persistent
G2 Chk1 Transient
No M-phase
S phase
G2 Chk1 Transient
G2 no Chk1
D
Aphidicolin
(0.5μM)
ATRi
45 cells
G2 onset
NEBD
1/FRET
S
G2
M
Time (min)
E
siControl
siTopBP1
Chk1 act.
in S phase:
High
Low
G2 onset
Time since G2 entry (h)
F
PARPi in S phase
% re-activation
in G2:
63.8
47.2
Chk1
re-activation:
PARPi
DMSO
No Chk1
re-activation:
PARPi
DMSO
S phase
G2 phase
1/FRET
Time since G2 entry (h)
G
Aphidicolin
(0.5μM)
Cdk1/2i
58 cells
Cdk1i
21 cells
Cdk2i
23 cells
G2 onset
1/FRET
S
G2
Time (min)
H
Plk1i in S phase
% re-activation
in G2:
64.5
21.0
Chk1
re-activation:
Plk1i
DMSO
No Chk1
re-activation:
Plk1i
DMSO
S phase
G2 phase
1/FRET
Time since G2 entry (h)

FIGURE 5

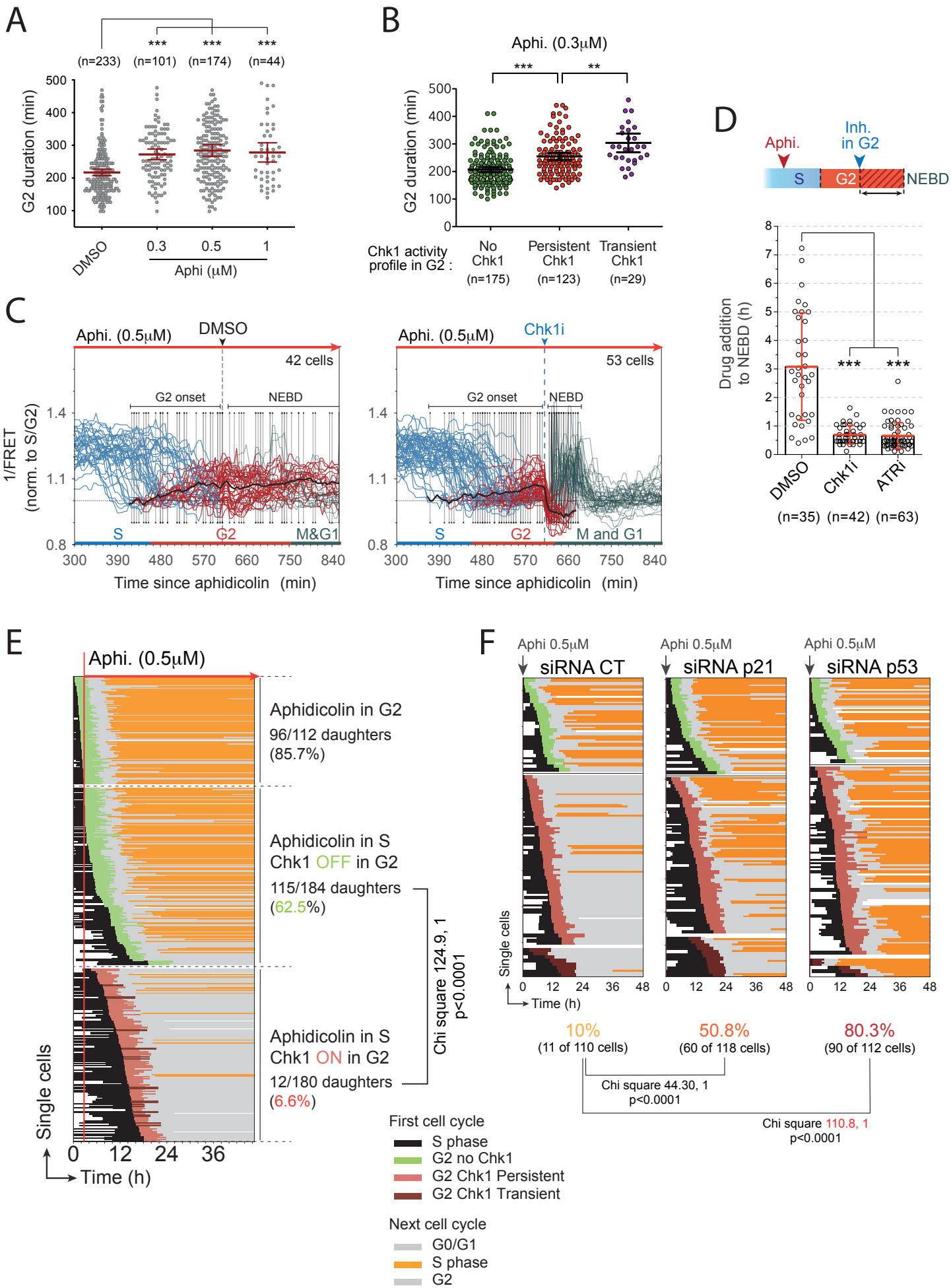
A
(n=233)
(n=101)
(n=174)
(n=44)
***
G2 duration (min)
DMSO
0.3
0.5
1
Aphi (μM)
B
Aphi. (0.3μM)
***
**
G2 duration (min)
Chk1 activity profile in G2 :
No Chk1 (n=175)
Persistent Chk1 (n=123)
Transient Chk1 (n=29)
C
Aphi. (0.5μM)
DMSO
42 cells
G2 onset
NEBD
1/FRET (norm. to S/G2)
S
G2
M&G1
Time since aphidicolin (min)
Aphi. (0.5μM)
Chk1i
53 cells
G2 onset
NEBD
S
G2
M and G1
Time since aphidicolin (min)
D
Aphi.
Inh. in G2
S
G2
NEBD
Drug addition to NEBD (h)
***
***
DMSO
Chk1i
ATRi
(n=35) (n=42) (n=63)
E
Aphi. (0.5μM)
Aphidicolin in G2
96/112 daughters
(85.7%)
Aphidicolin in S
Chk1 OFF in G2
115/184 daughters
(62.5%)
Aphidicolin in S
Chk1 ON in G2
12/180 daughters
(6.6%)
Chi square 124.9, 1
p<0.0001
Single cells
Time (h)
First cell cycle
S phase
G2 no Chk1
G2 Chk1 Persistent
G2 Chk1 Transient
Next cell cycle
G0/G1
S phase
G2
F
Aphi 0.5μM
siRNA CT
Aphi 0.5μM
siRNA p21
Aphi 0.5μM
siRNA p53
Single cells
Time (h)
10%
(11 of 110 cells)
50.8%
(60 of 118 cells)
80.3%
(90 of 112 cells)
Chi square 44.30, 1
p<0.0001
Chi square 110.8, 1
p<0.0001

FIGURE 6

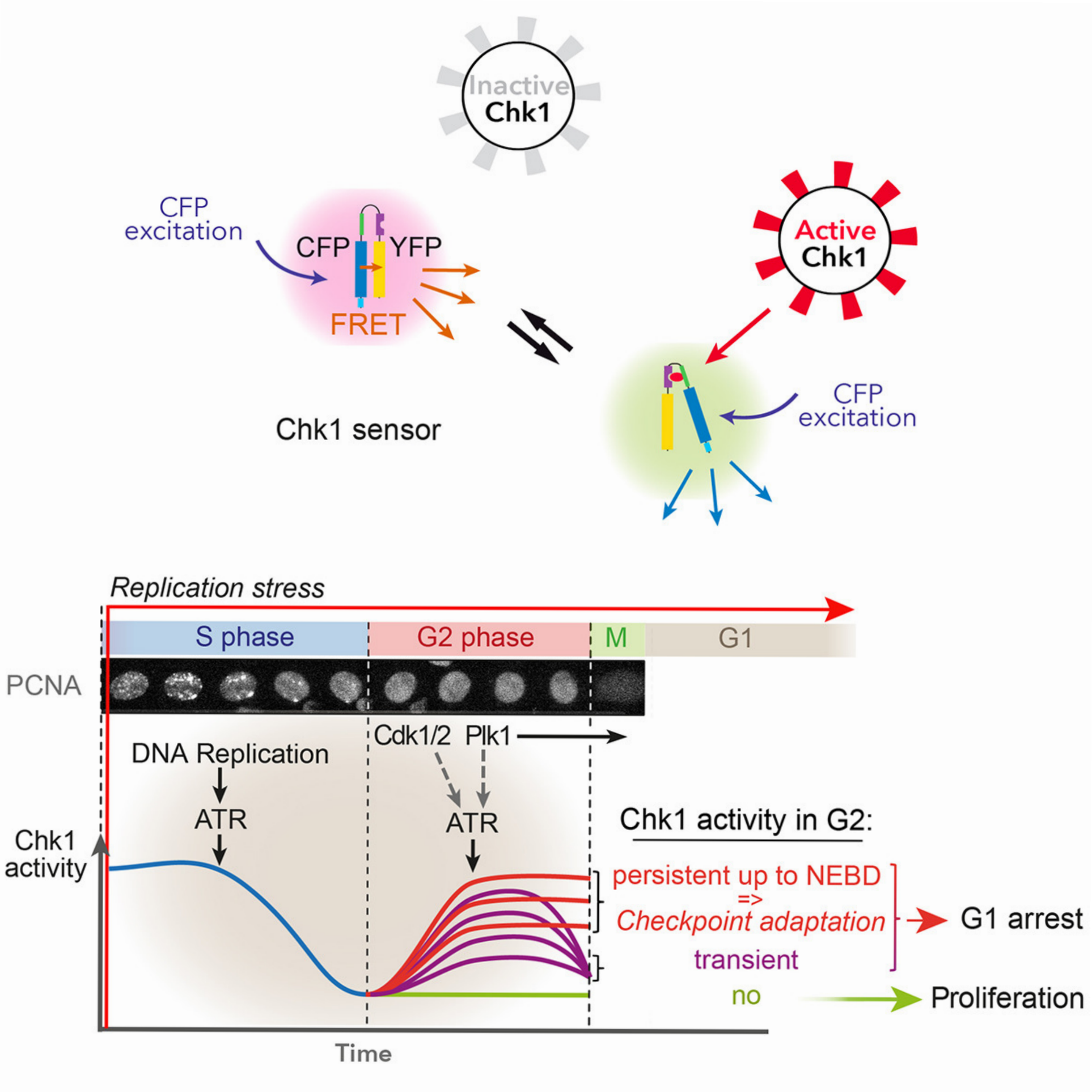
Inactive
Chk1
CFP
excitation
CFP
YFP
FRET
Active
Chk1
Chk1 sensor
CFP
excitation
Replication stress
S phase
G2 phase
M
G1
PCNA
DNA Replication
ATR
Cdk1/2
Plk1
ATR
Chk1
activity
Chk1 activity in G2:
persistent up to NEBD
=>
Checkpoint adaptation
transient
G1 arrest
no
Proliferation
Time